INTERNAL STRUCTURE OF POLY(OCTADECYL METHACRYLATE) LAMELLAE IN ORIENTED BLOCK COPOLYMERS

Santhosh Ayalur Karunakaran

Master thesis submitted in partial fulfillment to obtain

Masters of Science Degree in **Applied polymer Science**

from the

Department of Engineering Sciences

at the

Martin Luther University, Halle-Wittenberg

February 2006

Dedicated to my parents

Acknowledgements

My most sincere gratitude to **Prof.Dr.Gerhard Wegner**, Director, Max Planck Institute for Polymer research for giving me this opportunity to carry out this work.

I would like to thank wholeheartedly **PD Dr.Mario Beiner**, Dept. Of Physics, Martin Luther University, Halle-Wittenberg for leading me through every step and his constant support.

I thank **Dr. Ingo Lieberwirth**, Solid State Chemistry Group, Max Planck Institute for supervising this project.

My heartfelt thanks to **Prof. Dr. Jochen Gutmann, Prof.Dr. Manfred Wilhelm, PD Dr. Volker Enkelmann, Prof. Dr. Christoph Bubeck** for the several helpful discussions and for allowing to use their equipment.

I would like to thank **Dr. Claude Oelschlager** and **Dr. Susana Filipe** for helping do all shear experiments, specially the former without which no shear experiments would have been possible. Dr.Wojiceich Pisula is also thanked for helping do extrusion. I would like to reserve my words of thanks to Dr. Markus Wolkenhauer for the discussions that we had during the project.

I would like to specially thank the technicians **Michael Bach, Gunnar Glasser, Andreas Hanewald, Hans-Joerg Menges** for helping me do some of the experiments.

I would like to thank all my colleagues and co-workers in the institute for giving me a pleasant stay during my work.

Finally, I would like to thank The Almighty for helping me be what I am.

Table of Contents

Chapter 4

Results & Analysis

Chapter 5

Discussions

Chapter 6

Conclusions

Chapter 1

1.1 Introduction

Structure and crystallization of polymers is one of the widely studied branches of polymer science. Several aspects of crystallization have been studied so far, and one of them is the crystallization under confinements. For this, confined crystallization has been investigated inside porous glasses, zeolites, in thin films[1-4] etc., i.e inside geometries of dimensions of 10-1000 nm. Other than these above mentioned external confinements, studying crystallization confined in self-assembled nanostructures, i.e. in microphase separated block copolymers containing a glassy component have also been done[5]. In spite of differences, studying crystallization in block copolymers constrained by a glassy component is perceived to be similar to studying crystallization in thin films. In all of these above mentioned cases, significant changes have been observed in the kinetics and nucleation behavior of crystallization[6] and orientation of the crystallites[7].

So far studies of crystallization of block copolymers have mostly concentrated on main chain crystallizable polymers like polyethylene[8], poly(ethylenoxide)[9] etc. where chain folding plays a major role while side chain crystallization in block copolymers remains largely an unexplored field. A good candidate for a side chain crystallizing polymer is poly (n-octadecyl methacrylate) (PODMA) belonging to n-alkyl methacrylate family[10]. This polymer has an 18 membered crystallizable methyl side chain in each monomeric unit. It has already received sporadic attention for its crystallization, since the early days of polymer science with studies carried out with IR spectrsocopy[11],diffraction[12], dilatometry[10],dielectrics[12,13] etc. It has been recently shown[14] that the alkyl side chains form nano-domains driven by the immiscibility with the main chains, from where the crystallization proceeds. In this study, poly (styrene-block-octadecyl methacrylate) copolymers (P(S-b-ODMA)) in the microphase separated state is examined, where the polystyrene block, having a glass temperature (T_g) of about 90°C, remains glassy at temperatures when the side chains crystallize close to 30°C. Thus, this system is an excellent candidate to study side chain crystallization in a “strong confinement”, i.e. under conditions where the crystallization does not affect the block copolymer morphology.

1.2 Aim of this work

The packing of chains in side chain polymers like PODMA is still a point of discussion. From the earliest works, several structures have been proposed[11,12,15,58]. It is even more interesting to study the situation in a microphase separated block copolymer where additional constraints occur. Interestingly, the crystallization behavior of PODMA homopolymers and lamellar P(S-b-ODMA) block copolymers is similar. Crystallization kinteics and degree of crystallinity in small PODMA lamellae are only slightly affectd by the confinement[13].

There exists a hierarchy of lengths scales in the case of microphase separated P(S-block-ODMA) copolymer: the longest is the period of the copolymer domains in the range of a few 10's of nm. The intermediate length scale is the period of the lamellae formed by the intercalating side chains[12] and the main chains of PODMA in the range of a few nm. The shortest length scale is the classical crystalline packing of alkyl part of the side chains, in the range of few Å.

A more or less open point is the orientation of the different structural elements with respect to each other. The most natural picture which is predicted based on scattering data for unoriented samples is that the side chains pack hexagonally, the PODMA lamellae formed lie perpendicular to the block copolymer interface and that the side chains pack in a direction parallel to the block copolymer interface. It is the principal aim of the study to confirm this picture for one lamellar Poly(styrene-b-Octadecyl Methacrylate) (nomenclature:Lam20) sample and to quantify details.

The Objective of the study is:

- to orient the lamellar block copolymer using shear or other flow methods and find the orientation of the block copolymer lamellae
- to study the orientation of nanophase separated PODMA lamellae and the orientation of side chains in relation to the oriented microphase separated block copolymer morphology by scattering techniques (SAXS/WAXS) in order to prove or disprove existing ideas.
- to study in more detail the crystal packing and the crystal stem length using spectroscopic techniques (Raman).
- And finally, to propose a picture to show the internal structure of PODMA lamellae in oriented microphase separated P(S-block-ODMA) copolymers.

1.3 Outline of this thesis

Chapter 1 gives an introduction to the block copolymer system and a general introduction to the problem. The aim of the thesis is defined and the outline of the thesis is given.

Chapter 2 deals with the theoretical background which is required to understand the experimental work and the results in this thesis. In the first part, an introduction to block copolymers, the various self-assembling processes like crystallization and nano-phase separation that play a role in the final structure are discussed. In the second part, methods to prepare flow induced orientation of lamellar block copolymers are described. In the third part, a description of the fundamentals of the characterization methods that have been used in the study - 2D-Small angle X-ray scattering (SAXS) and 2D-Wide angle X-ray scattering (WAXS), Raman Spectroscopy and Scanning Electron microscopy including information that is required to evaluate the data is given.

Chapter 3, the experimental section, contains a description of the materials and methods used in this study; the system under study has been briefly described along with additional information about the synthesis and microstructures of the sample. Also, the various procedures adopted during the experiments along with the specifications of the instruments are given.

Chapter 4 is the results part. The X-ray scattering data of the shear oriented and extruded sample Lam20 along with a detailed analysis are given. Additionally, results from scanning electron microscopy for the two samples are included. In the next part, scattering results from another lamellar sample (nomenclature: LAM10) are given along with a detailed analysis. Results from Raman spectroscopy for the block copolymer sample Lam20 and the PODMA homopolymer Homo16 are given in the next part. The spectra are analysed and compared with the spectral analysis of n-alkanes which the side chains resemble.

Chapter 5 includes the discussion of all results. A simple model for the internal structure of the PODMA domains in lamellar P(S-ODMA) block copolymers is presented. Additional cases have been discussed to explain in part all other phenomenon including the various

cases of orientation of PODMA main chains and additional crystalline peaks. Results from Raman spectroscopy are also discussed.

Chapter 6 summarises the outcomes of the project condensely and suggestions are given for further work.

Chapter 2

Theoretical Background

2.1 Block copolymers

Block copolymers are segments of macromolecules covalently bonded. Tethering two of such segments together leads to what is known diblock copolymers that are a simple class of block copolymers. Other types include triblock copolymers, multi-block copolymers, star-block copolymers and more complicated structures.

Block copolymers find a wide range of industrial applications. In solid and rubbery states, as thermoplastic elastomers, they find their applications in impact modification, compatibilization and pressure sensitive adhesion. In solution, their surfactant properties are employed in foams, thickeners, oil additives and many more.

2.1.1 Microphase separation in Block copolymers

Like blends, block copolymers owing to the incompatibility of the constituent blocks tend to phase separate into separate individual domains in a wide temperature range. However, unlike blends that phase separate into domains that are as big as a few micrometres, block copolymers do not separate macroscopically due to the chemical bonds that inhibit such macrophase separation. Instead they self-assemble into various mesophases of sizes ranging from 5-50 nm depending on the length of each block in a process termed “micro-phase separation” (fig.2.1).

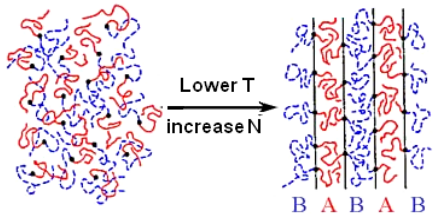

Figure 2.1 Microphase separation of a diblock copolymer.

The phase behavior of a block copolymer is determined by three individual factors: N, the overall degree of polymerisation, χ, the interaction parameter and f, the composition of the system that determines the volume fraction. Demixing in block copolymers is favoured by a decrease in free energy with demixing. The Gibb´s free energy of such a system is a sum of enthalpic and entropic contributions. It is related to the interaction parameter χ and the degree of polymerisation N by the following relation:

$$\Delta G = RT\left(\left(f_A/N_A\right)\ln f_A + \left(f_B/N_B\right)\ln f_B + \chi f_A f_B\right)$$

where f is the volume fraction of a component. The interaction parameter χ has a significant enthalpic contribution and is governed by the incompatibility of the blocks. The occurrence of N, the degree of polymerization, reflects the N-dependence of the entropic contributions. Additionally the interaction parameter is inversely proportional to temperature[16].

At equilibrium, the chains will be arranged in minimum free energy configurations. Increasing the interaction parameter by lowering the temperature favours reduction in contacts of different monomer. If N is sufficiently large, this effect is enhanced due to reduced entropy of mixing, and the tendency of the blocks to segregate to form mesophases increases. This process of segregation is called Microphase separation. Thus this process of microphase separation is parameterized using these two factors.

For any block copolymer system there exist a critical value of χN, at a given composition, i.e. at a given volume fraction, below which the block copolymer domains stay mixed. In the simplest case of a symmetric di-block copolymer (f=0.5), the transition from the demixed state to the mixed state occurs at a critical value of $\chi N=10.5$. Upon decreasing the temperature that results in an increase in χ, the degree of segregation can be increased. Depending upon the value of χN or in other words, the degree of segregation, three regimes have been found: Weak segregation limit or WSL (χN~10-12), intermediate (χN~12-100), and strong segregation limit or SSL ($\chi N > 100$).

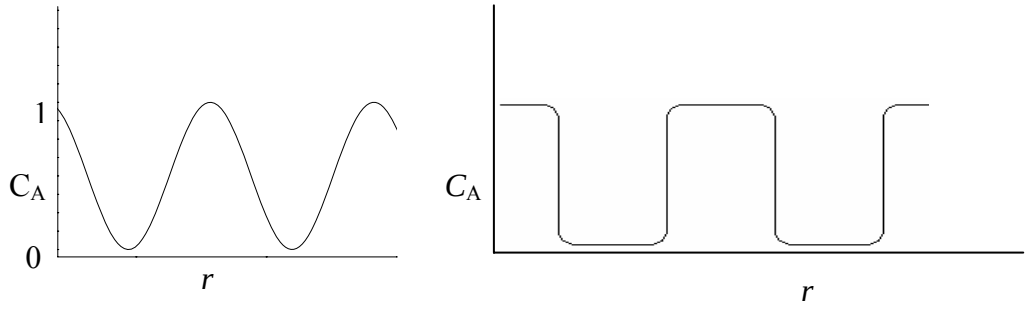

Figure 2.2 Composition profiles characterising the Weak Segregation limit (WSL) (left) and Strong Segregation Limit (right)[17] where C_A is the concentration of block A.

The limits are defined precisely depending on the criterion used, for e.g., the purity of each component in individual domains which increases on approaching SSL. In other words, these regimes give an idea of the composition profile of each component. In WSL, the composition profile is essentially sinusoidal whereas in the asymptotic SSL, the components are more pure and the interphase is narrow. The composition profiles of each

of the component in a diblock copolymer in the weak and strong segregation limit are given in Fig (2.2). The segregation in a symmetric diblock copolymer leads to planar interfaces. However, for block copolymers with largely differing volume fractions, the interfaces become more curved for energy reasons and different structures with curved interfaces are formed. A phase diagram for one of such systems indicating the different morphologies as a function of volume fraction is given in fig.2.3.

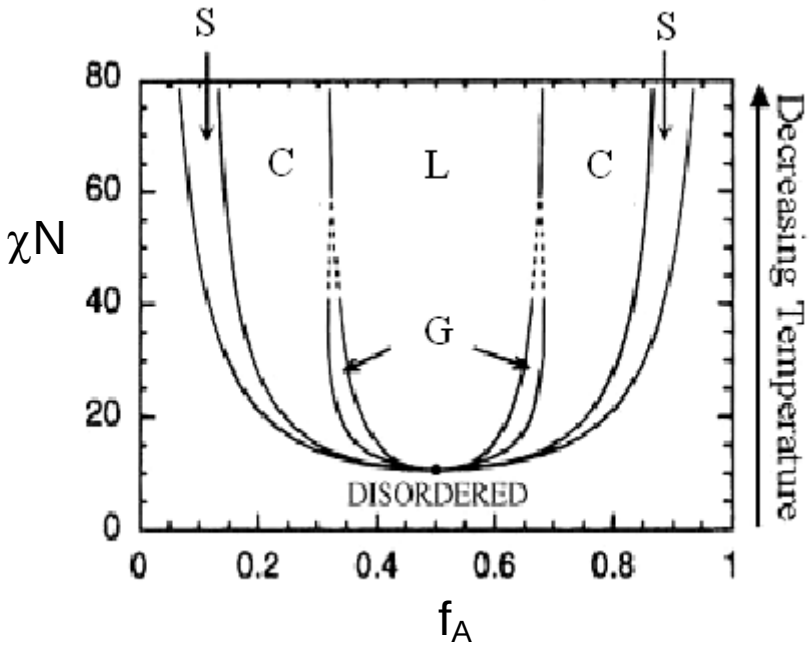

Figure 2.3 Theoretical Phase diagram of a diblock copolymer. (G-Gyroid, L-Lamellar, H-Hexagonally packed cylinder, S-Body Centred Cubically packed spheres)[18].

Fig. 2.4 gives a schematic sketch of some of the micro structures formed. The most important morphologies are lamellar, hexagonally packed cylinders and body centered cubically packed spheres. As seen below, by varying the volume fraction of one of the components we can achieve structures with either material as the matrix.

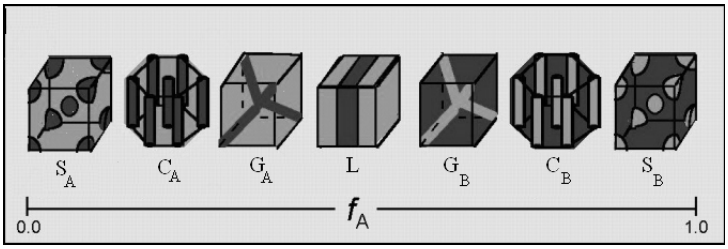

Fig 2.4 Different microstructures formed upon variation of volume fraction of one of the components. The subscript denotes the minor component[17].

Apart from the structures discussed above, other more complicated structures like the Hexagonal modulated lamellar(HML), hexagonal perforated layer (HPL) have been sometimes observed in small regions of the phase diagram between lamellar and the hexagonal packed cylinder phase boundaries.

2.1.2 Crystallization in Block copolymers

The final structure of a block copolymer that has a crystallizable block does not only depend on the microphase separation process driven by the incompatibility of the two blocks but also on the crystallization of one of the blocks[19]. The final structure is a result of the interplay of several factors during crystallization. Different situations have been reported in the literature so far. Especially "strong confinement" and "break-out behavior" has been discussed.

Strong confinement is characterized by a block copolymer morphology which remains nearly unaffected during/by crystallization while "break-out behavior" is related to a complete change in the block copolymer morphology after crystallization. For systems, where the glass temperature of the amorphous phase (T_g(A)) is much higher than the crystallization temperature(T_c(B)) i.e. $T_g(A) >> T_c(B)$, crystallization occurs usually in a "strong confinement". In cases where $T_g(A) \sim T_c(B)$, strong confinement or break-out crystallization behavior seem to depend on the degree of segregation between the two blocks. In any case, there is interplay of thermodynamic forces and kinetic hindrances. Some examples are discussed below:

In poly(ε-caprolactone-b-butadiene)[20], crystallization was found to destroy already formed microdomains in the melt in samples with $T_{ODT} \sim T_c$. While in samples with $T_{ODT} < T_c$, microphase separation was not even observed. Also in the case of Poly(ethylene-ethylene/propylene) (PE-PE/P)[21] , it has been shown that for all compositions (12-56 wt% PE), final morphology is always lamellar. This has been interpreted that the microphase separation does not influence the structure formed by crystallization. Ryan etal[22], who examined a series of block copolymers, whose T_{ODT} was not so high compared to the T_c found that crystallization from an organized melt destroyed the melt morphology resulting in a lamellar structure. Block copolymers of Poly(ethylene-3-methyl-1-butene) (P(E-b-MB)) with different molecular weights, i.e. with different segregation strengths have also been studied[23,24] previously. In case of samples with low segregation strengths,

crystallization is strong enough to disrupt the morphology while it did not have a major effect on the melt morphology in highly segregated system.

Based on all these observations, it has been elucidated that such break-out crystallization depends on the segregation strength for block copolymers with a rubbery chain as the amorphous component.

Crystallization in confinements occurs in well-segregated samples and in samples with glassy components. In copolymers with glassy components[25-31], confinement effects are observed due to freezing-in of the melt morphology even if the system is weakly segregated. In such cases, the kinetics of crystallization was largely affected. Confinement effects observed in well-segregated systems[23,24] due to high energy of mixing allow the microphase separated morphology to be strong enough not to be disrupted by crystallization.

A strong contrast between confinements observed due to the presence of glassy matrix and degree of segregation is that the crystallization kinetics is affected differently in each case. In the case of glassy matrix, crystallization is homogeneously initiated, and the kinetics is more first-order rather than sigmoidal, as conventionally observed during polymer crystallization. While in the latter case of strongly segregated systems with rubbery amorphous component, crystallization follows sigmoidal kinetics which is not as different as in the case of weakly segregated diblocks, where crystallization changes the melt morphology.

Thus it is not only of interest to see how the crystallization affects the melt morphology, but also how crystallization is affected by constraints. Several studies have concentrated on this problem. In analogy to studying crystallization in block copolymer confinements, crystallization has also been studied in thin films of thicknesses 10-1000 nm[32,33], in small droplets on surfaces produced by dewetting from thin films[34,35] and in other confinements like nanoporous glasses[36]. It has been shown in all cases, that when crystallization is confined in such strong confinements, significant effects are seen in the kinetics, the nucleation behavior and morphology. However, practically all studies discussed above deal with the crystallization of long main chains under confinements where chain folding plays a major role. In case of microphase separated P(S-b-ODMA) block copolymers studied in this work, it is the long alkyl groups in side chains that undergo crystallization in strong confinements.

2.1.3. Side Chain crystalline Block copolymers:

Crystallization of side chains in block copolymers or in confinements have not been studied so far in great detail. It is now understood[14] that in the case of side chain polymers with long alkyl groups, alkyl nanodomains are formed due to incompatibility of the side chains and main chains. It is from these preformed alkyl domains do crystallization occur. A consequence of the existence of such alkyl nanodomains in block copolymers is a hierarchy of two length scales: one due to this nanophase separation in the range of 2-5 nm, and the other due to microphase separation of the two blocks in the scales of 10-50 nm.

Block copolymers containing higher n-alkyl methacrylate or higher n-alkyl acrylates belong to this category. Nanophase separation occurs due to the incompatibility of methacrylate main chains and the long alkyl groups in the side chains. It has been shown that for methacrylate and acrylate series, the members with C>4, where C is the number of alkyl carbons per side chain, are able to form separate alkyl nanodomains. These members show a polyethylene like glass transition called α_{PE} originating from these nanodomains in addition to the conventional glass transition[14]. Approaching C~12, the side chains of atactic samples start to crystallize. Somehow this side chain crystallization can be discussed as crystallization of frustrated alkanes.[37]

PODMA or Poly(Octadecyl Methacrylate) is a member belonging to the family of n-alkyl methacrylates with crystallizable side chain containing 18 carbons. PODMA homopolymers do crystallize at 30°C in a DSC cooling experiment (with a rate of -10K/min). PODMA has been of considerable interest for its crystallization[38,39] and has sparked debates upon its packing[15,58] . The way these chains pack has received considerable attention from several groups, and has been investigation by Raman spectroscopy[11], X-ray scattering[12], Dielectrics[12,13], Calorimetry[40] etc. Based on these studies it has been concluded that around twelve methylene groups typically stay in the amorphous state in PODMA[13] and has been shown that these side chains exist in an inter-digitating fashion[12].

Poly (styrene-Octadecyl Methacrylate) block copolymers of varying volume fractions were investigated recently[40]. As expected, effects of confinements were well seen on systems with small cylindrical PODMA domains in the form of reduced degree of crystallinity, changes in the nucleation behaviour and slowing down of the crystallization

kinetics. Lamellar copolymers however behaved more or less the way homopolymers behave, especially ones with large domain size.

Here in this study, a lamellar system is investigated using scattering techniques in order to elucidate the structure and orientation of the side chains and the main chains with respect to each other and the way they exist in the block copolymer. Further details about the packing and conformational details of the side chain in crystalline state are also of interest. Spectroscopic techniques are applied to get information on this, since scattering techniques are less informative in these special systems.

2.2. Flow Induced Orientation of Block Copolymers

2.2.1. Shear Orientation

Owing to the ease with which defects are created in soft materials like block copolymers, it is difficult to prepare block copolymers in a macroscopically oriented state. Macroscopic orientation helps us to get more insight into the structure like in the case of a single crystal. The application of large amplitude oscillatory shear (LAOS) in the non-linear regime to lamellar block copolymers has proven to be a very effective method to induce long range order in lamellar block copolymer (fig.2.5.) and hence has been of considerable interest in the recent years.

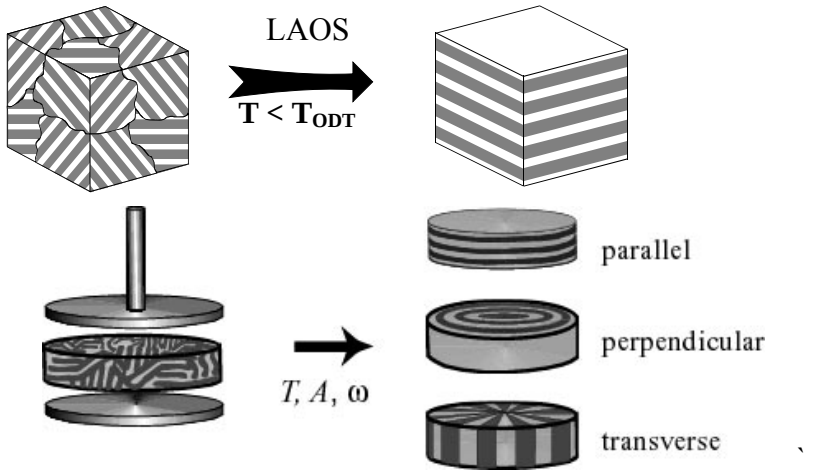

Figure 2.5 Sketch illustrating the effect of LAOS on isotropic lamellar block copolymers (upper part) and the three possible orientations observed during shearing (lower part)[46]

Pioneered by keller etal[41] the effect of mechanical field on orientation has attracted a lot of attention[42,43] though alternative methods like electric fields[44] and more recently

magnetic fields[45] exist. In addition to studying orientation, shear fields are also a useful tool to study order-disorder phenomenon and order-order transition in block copolymers.

In general, upon the application of LAOS, three different types of orientation of the block copolymer lamellae have been observed: (i) Parallel orientation, where the layer normal lies parallel to the shear gradient and perpendicular to the shear direction; (ii) Perpendicular orientation, where the lamellae normal is oriented perpendicular to the shear gradient and shear direction, and in rare cases; (iii) Transverse orientation, where the layer normal lies perpendicular to the shear gradient and parallel to the shear direction (fig 2.5)[47] Initial studies reported only parallel orientation of lamellae. Only later on, perpendicular orientation was observed. Transversal orientation has been observed only to be a transient case between unoriented and parallel oriented state.

Koppi etal.[48] studied dynamics of orientation to show the frequency-dependent behavior of orientation. Zhang etal.[47] confirmed the findings and concluded that at very high and low frequencies, parallel orientations could be achieved while at intermediate frequencies, perpendicular orientation could be observed.

Chen etal[49] in order to explain the frequency dependant alignment behavior, proposed two characteristic frequencies: ω_c, above which the distortion of chain conformations dominate the material's viscoelasticity, and ω_d, frequency below the relaxation of domains become more significant. Based on this they proposed a phase diagram, explaining the behavior shown in fig.2.6.

Four different frequency regimes were identified where different orientations dominate. Perpendicular orientation dominates at frequencies too fast for domain relaxation but slow enough for chain conformations to relax i.e $\omega_d < \omega < \omega_c$(Regime I). Shearing at frequencies above ω_c results in parallel orientation in two different paths.

At frequencies just above ω_c, a transient (bimodal) orientation distribution consisting of parallel and perpendicular orientation as well as a range of orientation between them (regime II) is observed. In contrast, for $\omega >> \omega_c$, parallel orientation resulting from a bimodal orientation of parallel and transverse orientations was observed (regime III). At all low frequencies, parallel orientation was observed (regime IV).

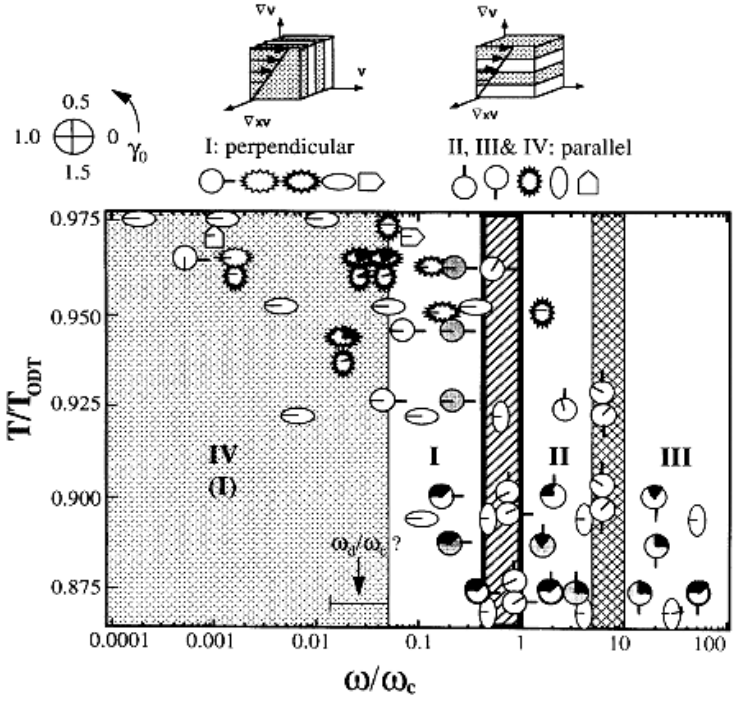

Figure 2.6 Phase diagram proposed by Chen et.al showing different frequency regimes resulting in different orientations.

Lately, computer simulation[50] added vital parameters which have so far been neglected: layer thickness and surface interactions of the lamellae. Despite all these studies, the understanding of shear induced orientation seems far from complete and further experimental and theoretical research is going on to understand the science behind this.

2.3. Experimental techniques

2.3.1. Two dimensional Small Angle and Wide Angle X-ray Scattering

X-rays are electromagnetic waves produced by targeting electrons to strike a metal like Cu, Fe or Mo kept at high vacuum and electric potential. If the colliding electron has enough energy, it knocks out another electron from the inner shell of the metal atom. As a result, a vacancy is created and to fill this vacancy, electrons from higher energy levels come down to this level. The energy difference between the two levels is then emitted as an X-ray photon. X-rays have a wavelength of about 0.1 Å to 100 Å which lies in the same range as that of the bond length and distances between the atoms in condensed matter, and hence finds its use in exploring structures in crystalline and soft materials.

X-ray scattering is an experimental technique that exploits the fact that X-rays are scattered by electron clouds which causes an interference pattern. Its special usefulness in the study of periodic structures lies in its ability to distinguish between regions of varying electron density which is usually the case in semi-crystalline polymers as well as block-copolymers. Thus, X-ray scattering is a powerful tool to study polymeric systems.

When a sample is irradiated with X-rays, they are scattered from different scattering centers. When there are interactions resulting in change of energy in X-rays leading to change in phase, the process is known as incoherent scattering. However, this is not of interest for our discussion since it is the coherent scattering, where there is neither a phase change nor an energy change during the interactions that bears information on the crystal structure. When plane incident waves are coherently scattered, the emanating secondary waves undergo interference. The waves can constructively interfere resulting in high intensity when they are in phase. For this to occur, the path difference between the waves originating from different scattering centers must be an integral multiple of wavelength which can occur only for specific scattering angles. The angle at which constructive interference will occur depends on the distance between the scattering centers. Thus, this distance can be uniquely determined knowing the angle of scattering and the wavelength λ of the radiation. In the case of a crystal, the inter-planar distance or the distance between the planes which are involved in scattering can be determined from the position of the peak maxima of the scattering intensity. This relationship is given by "*Bragg's Law*" which is derived below.

Consider that a plane incident wave traveling in the direction characterized by the vector S_0 is scattered by particles at points O and P. The secondary spherical waves are collected in a direction specified by the vector S. When there is no phase change involved during this process, the phase difference $\Delta\phi$ between the waves scattered at O and P and arriving at the detector depends only on path difference δ according to

$$\Delta\phi = 2\pi\,\delta / \lambda \qquad (1)$$

where λ is the wavelength of the X-ray radiation used.

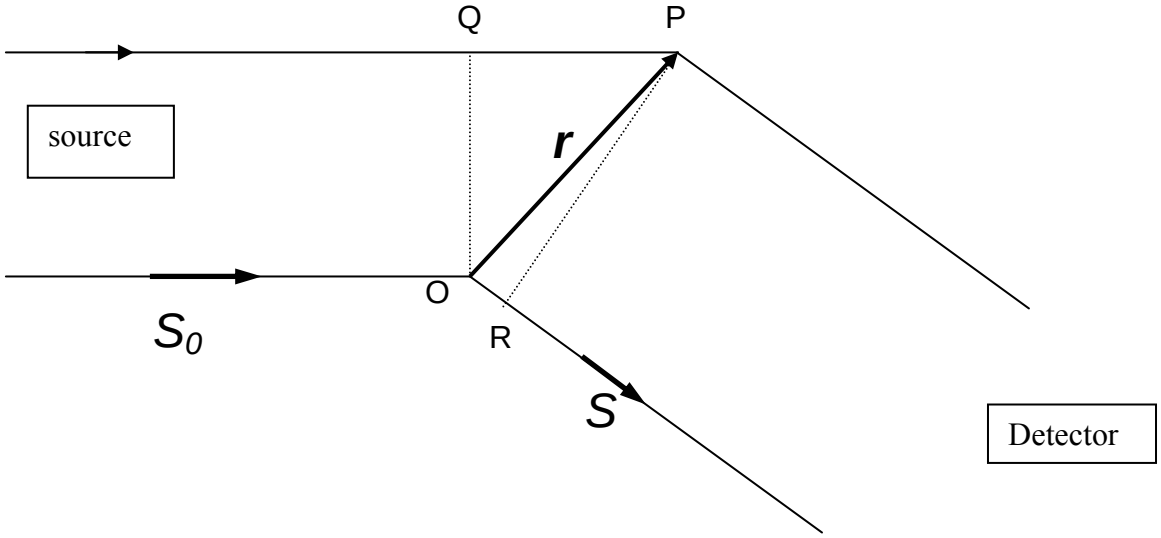

Figure 2.7 Geometry showing the Path Length difference

If vector r designates the position of point P with reference to point O, we have QP=<$\underline{S_0}.\underline{r}$> and OR=<$\underline{S}.\underline{r}$>, and the path difference is: QP-OR

And the phase difference $\Delta\phi = 2\pi\ (<\underline{S_0}.\underline{r}> - <\underline{S}.\underline{r}>) / \lambda$

$$= -2\pi \underline{s}\ .\underline{r}$$

where $\underline{s} = \underline{S}-\underline{S_0}/\ \lambda$ (2)

The vector *s* is referred to as the scattering vector and it completely characterizes the scattering geometry: the incident and the scattered beam directions and the wavelength. Its magnitude is given by

$$|\underline{s}| = s = 2\ \sin\theta\ /\ \lambda \quad (3)$$

where 2θ is the scattering angle or the angle between the incident and the scattered beams. If *d* is the distance between the scattering centers, it is related to s by:

$$s = 1\ /d \quad (4)$$

substituting this into (3) gives the relation between the scattering angle 2θ and the inter-planar distance d :

$$2d\sin\theta = \lambda \quad (5)$$

This is Bragg's Law connecting the characteristic length d of a periodic structure with the scattering vector *s*, which is in some cases also defined as $q = 2\pi s$

For experimental and theoretical reasons, X-ray diffraction is classified as SAXS and WAXS for Small angle and Wide angle scattering depending on the angle of observation. From Bragg's equation, we see the reciprocity between the inter-planar

distance d and the angle of scattering θ, which means that inhomogeneties of mesoscopic dimensions are observed at small angles typically 2θ < 2°,while inhomogeneties of atomic dimensions give rise to large angle scattering.

Generally, untreated polycrystalline materials are isotropic, without any preferred orientation of the crystallites. The diffractrogram of such polycrystalline materials with random orientation gives rise to what is known as 'powder pattern' that consists of a series of concentric rings with each ring corresponding to a Bragg reflection d_{hkl}. On the other hand, the diffraction pattern of an ensemble of oriented crystallites is no longer concentric circles, but arcs or ideally intense points. The length and orientation of the arc depends on the extent of orientation and the direction in which the normal to the diffracting planes are oriented respectively. Thus in the case of samples where orientation is of prime importance, 2D-detectors (a.c.a. area detectors) need to be used. Figure 2.8 explains the information that is procured from Area detectors.

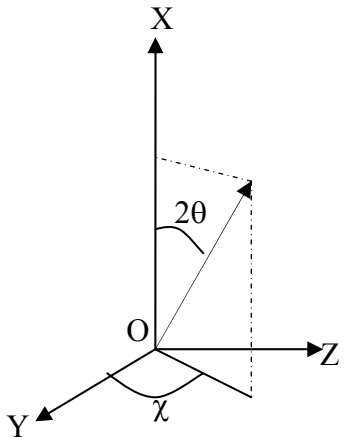

Figure 2.8. Geometry showing the scattering angle(2θ) and pole angle (χ). The incident beam travels along X-axis and O is the scattering centre.

In the case of normally used detectors like a kratky camera, we get information on intensity as a function of the scattering angle (2θ) only. Upon using an area detector, we get information about the intensity as a function of the angle of scattering (2θ) as well as the azimuthal angle (χ) which gives information about orientation. In order to visualize the azimuthal dependence of a certain reflection, the intensity from such 2D-scattering experiment can be integrated upon a particular range of scattering angle 2θ corresponding to the reflection.

For the identification of orientation of lamellar block copolymers, 2D-SAXS has proven to be a suitable technique. We can identify the type of orientation of the lamellae

by studying the contributions from three orthogonal views namely: normal, radial and tangential. Normal View is defined as the view that runs along the shear gradient or along the cylinder axis. Radial view is defined along the vorticity or along the diameter and Tangential view is defined along the shear direction or along the tangent drawn to the diameter.

In the normal view of parallel oriented lamellae (see fig.2.5), the normal to the diffracting planes, that is the normal to the lamellae, lies in the same direction as the view and hence there is no specific orientation contribution in this view.

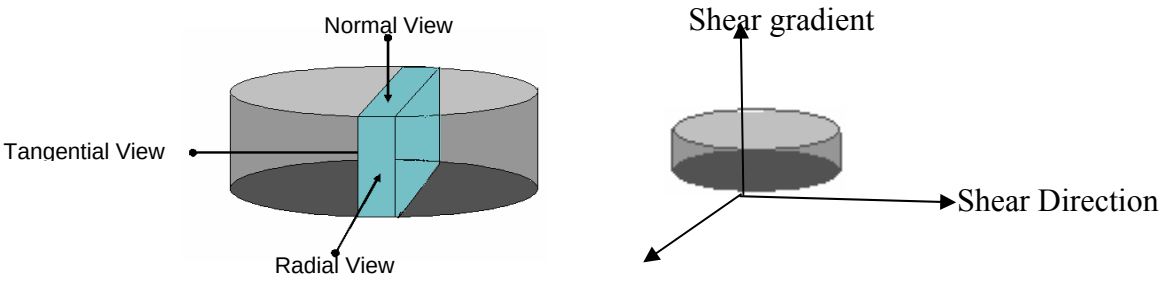

Figure 2.9 Sketch showing the three orthogonal views to identify orientation (right). The various labels used in identifying the different views are given alongside (left).

However in the tangential and the radial view, the layer normal lies perpendicular to the view. Thus parallel orientation is identified with low intensity and isotropic contributions in the normal view and strong anisotropic contributions in the radial and the tangential view as shown in fig 2.10.

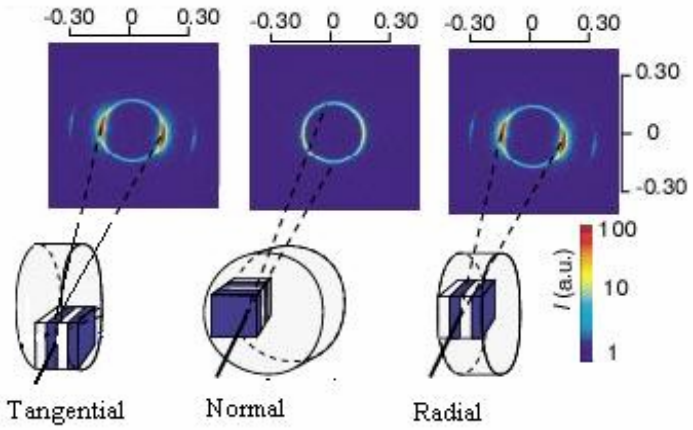

Figure 2.10. Model 2D-SAXS patterns for a parellely aligned block copolymer lamellae. The intense anisotropic contributions in the tangential and radial views and isotropic contributions (circle) in the normal view[46].

For similar reasons, perpendicular orientation (as in fig.2.5) is identified with intense peaks in the tangential and normal views and weak isotropic contributions in the radial view.

Transverse, the other possible orientation is identified with strong anisotropic contributions in the normal and radial view and weak isotropic contributions in the tangential view.

2.3.2. Scanning Electron Micropscopy:

Scanning Electron Microscopy (SEM) uses a beam of focussed electrons to examine objects on a very fine scale giving information about topography, morphology and composition.

A beam of electrons, focused using metal apertures and magnetic lenses into a thin monochromatic beam is accelerated towards the specimen using a positive potential resulting in interactions between the irradiated sample and the electron beam. These interactions result in the production of backscattered electrons, secondary electrons, X-rays etc. A schematic sketch of a scanning electron microscope is given below in fig. 3.6.

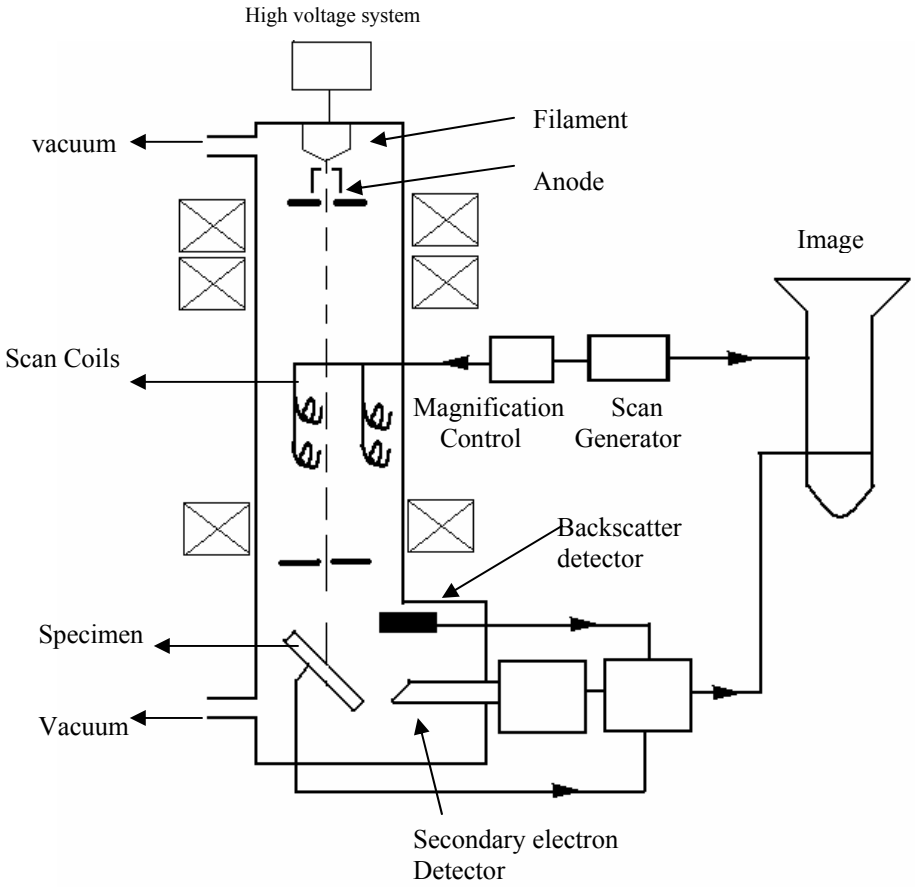

Figure 3.6. A schematic sketch of a Scanning Electron Microscope (SEM)

Secondary electrons are produced when an incident electron excites an electron in the sample and loses some of its energy in this process. The excited electron moves towards the surface of the sample undergoing elastic and inelastic collisions until it reaches the surface, where it can escape if it still has sufficient energy.

Thus, they have relatively low energy of less than 50 eV and hence can be emitted from a few nm of the top surface. Increasing the surface area that interacts with the beam, results in the increase of the secondary electron emission.

Backscattered electrons are primary beam electrons that have been inelastically scattered within the sample and escape from the surface. The fraction escaping varies from 0.06 (for carbon) to 0.5 (for gold), i.e. recording backscattered electrons gives information about compositional contrast in the specimen. They have high energy and can come from depth upto 1μm.

Separate detectors positioned at different places inside the chamber, detect the secondary and backscattered electrons emitted from a point due to interaction. A collective image is formed by scanning the whole surface of the sample and the contrast of the image is given by the intensity of the detector signal.

2.3.3. Raman Spectroscopy:

Photons are able to interact with molecules and can induce transitions between different molecular energy states. This is the basis of vibration spectroscopic techniques like IR spectroscopy and Raman scattering detecting transitions between different vibrational states. The energy gaps between different states ($\Delta E=h\nu$) correspond in this case to frequencies ν in the IR range**.** The scattering of the photons involving no transfer of energy between the incident photon and matter, a process known as Elastic or Raleigh scattering. If the scattering event involves some transfer of energy, this process is Inelastic and called Raman scattering. The energy transfer of Raman scattering is related to a transition between different vibrational states of the molecules. However the probability of the occurrence of Raman scattering is as less as 1 in 10^7. Typical applications of Raman spectroscopy are in structure determination, multi-component qualitative analysis, and quantitative analysis.

In the process of Raman scattering, the incident photon could transfer energy to the molecule and excite it to a higher vibrational state than the non-vibrational ground state. This is called stokes scattering. On the contrary if the incident photon gains energy from

the molecule in which the molecule goes to a lower energy state, the scattering is called Anti-Stokes Scattering.

Raman spectroscopy measures the wavelength and intensity of these inelastically scattered photons. The Raman scattered light occurs at wavelengths that are shifted from the incident light by the energies of molecular vibrations.

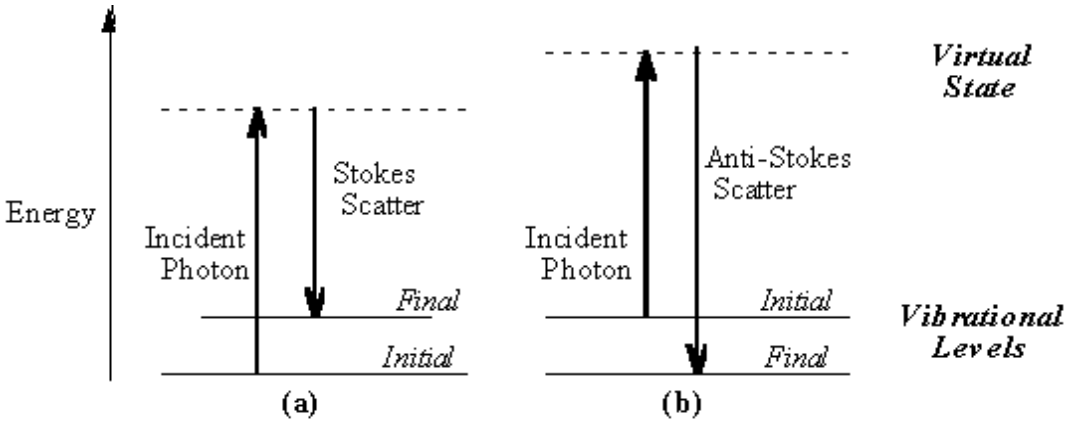

Figure 2.11. Various transitions involving Energy Transfers.

The mechanism of Raman scattering is different from that of infrared absorption, and Raman and IR spectra provide complementary information. Raman scattering occurs only in cases where the molecular vibration changes the polarizability of a molecule. This serves as the selection rule for a vibration to be Raman active.

The intensity of a Raman scattering is

$$I \alpha (\delta\alpha / \delta Q)^2$$

Where α is the polarizability, and Q- normal coordinate of the vibration. Thus any vibration involving no change in polarizability is invisible in Raman Spectra.

The Raman spectra of solid n-alkane exhibits a characteristic set of bands composed of a strong fundamental and a number of overtones in the low-frequency region. Valid only for carbon atoms arranged in trans conformation, these bands reflect the symmetrical accordion type longitudinal vibrations of the chains. These vibrations are identical to the longitudinal acoustic standing waves and hence the name longitudinal acoustic mode (LAM) is used. It has been observed that the frequency shift is inversely proportional to the number of carbon atoms in the trans conformation in the crystallite.

Previous studies[51,52] have been successful in using this technique to evaluate the crystalline stem length in n-alkanes and cyclic alkanes. According to Strobl etal.[55] the stem length can be calculated by:

$$\nu_{LAM} = 2236 / (n-1.6) + 2.2$$

where ν_{LAM} is the Raman shift, and n the no. of methylene groups in the crystallite stem. Thus, by knowing the frequency of LAM, if existing, one can calculate the crystal thickness.

For n-alkanes[51], a peak at 1080 cm^{-1} has been assigned to the gauche conformers in the non-crystalline state. Information on the kind of packing can also be obtained by observing certain peaks. For e.g. a band at 1417 cm^{-1} is observed for orthorhombic crystals in crystalline polyethylene. In case of hexagonally packed cyclic alkanes, a narrow band at 2850 cm^{-1}, a broad band near 2898 cm^{-1} and a weak shoulder at 2931 cm^{-1} is observed. With the help of these specific bands, one can also get supporting evidence for the type of packing.

Chapter 3

Experimental Section

3.1. Materials

3.1.1 Synthesis of Poly(styrene-block-Octadecyl Methacrylate)

The investigated Poly(Styrene-b-Octadecyl methacrylate) and the Poly(Octadecyl methacrylate) polymers were both synthesized using anionic polymerization technique using commercial monomers of high purity. Complete details of the materials, methods, and equipment used for the synthesis can be found elsewhere[13].

3.1.2. Sample Characterization

Size exclusion chromatography was used to determine molecular weight parameters. The composition was determined based on ^{1}H-NMR measurements. For the volume fraction calculations, (ρ_{PS}=1.04 g/cm3 and ρ_{PODMA}=0.865 g/cm3) were used as the densities of homopolymers of Styrene and Octadecyl methacrylate respectively. The copolymer morphology and PODMA domain size were studied using X-ray scattering techniques. The samples showed lamellar ODMA domains. The calorimetric data and other important thermal data including glass transition temperature (T_g) of PS, melting temperature (T_m), crystallization temperature (T_c) as well as the degree of crystallinity of the ODMA constituent of the copolymer were obtained from DSC measurements. The most important characterization data is given below in table 3.1 below. The difference in the characteristic temperatures of the various components for e.g., the T_g of PS arises from the varying domains sizes and block lengths between the samples.

Table 3.1 Characterisation data for the investigated samples

Sample	N_{PS}	N_{PODMA}	M_n (Kg/Mol)	d_{ODMA} (nm)	Φ_{PODMA}	T_g^{PS} (°C)	$^{\dagger}T_m^{PODMA}$ (°C)	$^{\dagger}T_c^{PODMA}$ (°C)	D_{DSC} (% mol)
LAM 20	257	52	44.3	16.6	0.44	91	30	24	27
LAM10	154	25	24.4	8.9	0.39	84	28	22	25
HOMO16	-	16	8.7	-	1	-	30	24	30

N - Degree of polymerisation of the component
d - Thickness of the PODMA lamellae
Φ -Volume fraction of the component.
† - Onset temperature of crystallization/melting as observed by DSC at (+/-)10K/Min.

3.2 Orientation of Block copolymer Lamellae

In this section, the procedure adopted for orienting lamellar P(S-b-ODMA) block copolymers using flow methods is described in detail.

3.2.1 Shear Orientation:

Shear orientation experiments were done in an Rheometrics ARES rheometer (torque range : $4*10^{-7}$ - 0.1 Nm) fitted with a IKFRTN1 torque transducer. Calculated quantity of the sample in the form of powder was pressed at 130°C into a disc of diameter 8mm and a thickness of 1 mm in a die for 15 minutes and then a pressure of 20 bars was applied for the same time. The pressed samples were then allowed to microphase separate by annealing the sample at 150°C for 24 hours in Vacuum.

Table 3.2 Various Shear Programs for the samples Lam20 and Lam10

Sample	Label	Temperature (°C)	Strain amplitude (%)	Frequency (Hz)	Time (Hrs)
Lam20	Rheo I	130	50	0.1	10
	Rheo II	130	100	0.1	10
	Rheo III	150	100	0.1	8
	Rheo IV	150	150	0.1	8
	Rheo V	170	150	0.1	8
Lam10	Rheo I	130	50	0.1	10

This microphase separated sample was equilibrated at the shear temperature for ½ hour before shearing. It was then sheared between two parallel plates of diameter 8mm in nitrogen atmosphere. The different programs adopted are given above in table 3.2. After shearing at elevated temperatures, the sample was cooled down to room temperature with a rate of about 10 K/min. All subsequent experiments with SAXS/WAXS and other techniques were done on samples stored at different periods at room temperature before measurement.

3.2.2 Extrusion:

Extruded samples were prepared on a home-made extruder with a die diameter of 0.7 mm. The Extruder has a die connected to a barrel of larger diameter with the whole apparatus heated by a copper heater jacketing it completely. A schematic sketch of the extruder is given in fig. 3.8.

The extruder cylinder is filled with approx. 20-30 mg of the microphase separated sample and heated to about 130°C in about 3 minutes. Then, the sample was manually extruded in less than 30 seconds. A typical length of the fibre is about 40 mm.

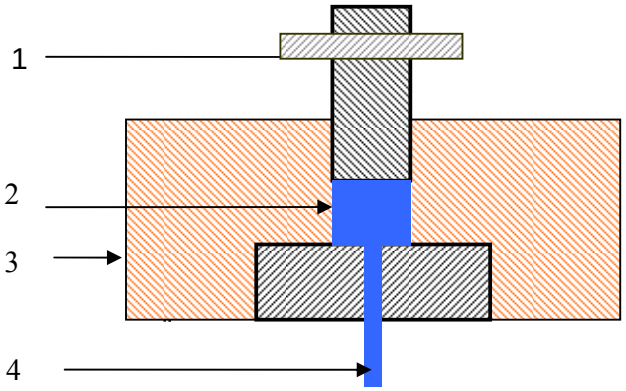

Figure 3.8 Cross–Section of the extruder showing 1. Plunger 2. Loading cylinder 3. Jacket Heater with 4. Fiber extruding through the pore of the die.

After extrusion, due to contact with atmosphere, the samples are quenched to room temperature rapidly from the extrusion temperature. It is important to note that the setup is unsophisticated which makes it very difficult to characterize further parameters.

3.3 Structure Determination

3.3.1 2-Dimensional Small angle and Wide angle X-ray Scattering

2D-Small angle and 2D-Wide Angle X-ray diffraction measurements were performed with a rotating anode (Rigaku 18 kW) X-ray beam with a pinhole collimation and a 2D Siemens detector with a beam diameter of ca. 1 mm. A double graphite monochromator for the Cu-K_α radiation (λ=0.154 nm) was used.

A small cube of size 1x1x1 mm^3 was cut from the shear oriented sample along halfway through the radius. Fig.3.9 explains this more clearly.

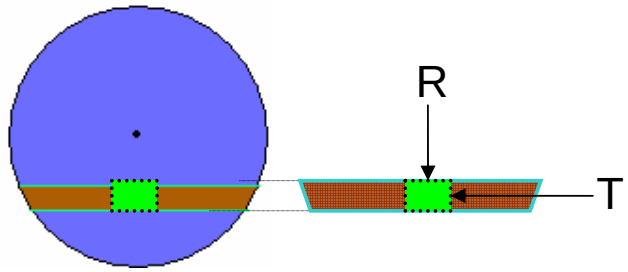

Figure 3.9. Sheared sample (top View) and the part of the sample measured. The direction of tangential and radial views can also be seen marked by arrows. The direction of normal view lies perpendicular to the plane of the paper.

For technical reasons, only the region of the sample shown above is selected for measurements although the effective shear would be a function of the distance from the centre to the point of measurement. Measurements were made on the three orthogonal directions as shown in fig.2.9.

The samples were measured in the transmission geometry at room temperature (23±2°C) mounted on a tape whose contribution was subtracted from the original contribution. All of the measurements were made for an exposure time of 1 hour.

In the case of temperature dependent WAXS measurements, a home-build heater with a normal temperature control device fitted with PT-100 sensor was used. Lower temperatures were achieved using liquid nitrogen supply controlled by the same heater, and a separate supply of nitrogen gas was used to take away any moisture forming. The temperature difference between the set and experimental temperature or the error is estimated to be in the range ± 2° C.

As much as possible, the position of the sample with respect to the beam in both the measurements is tried to be kept the same so that the orientations in the two measurements remain comparable. However significant uncertainties are expected under these experimental conditions (± 5°).

3.3.2 Scanning Electron microscopy

Scanning electron micrographs were obtained on a Leo Gemini 1530 SEM. Scans on the fibers were made on the plane perpendicular to the fibers axis. Scans on the sheared sample were made on the planes that are viewed in the tangential/radial views. The views are made with a tilt of 15° with respect to the beam for technical reasons.

3.3.3 FT-RAMAN Spectroscopy

Raman scattering measurements were made on a commercial BRUKER RF 100/S Raman Spectrometer. All measurements were made at room temperature in reflection geometry by filling the crushed sample into a hemi-spherical cavity (diameter 1.5mm) drilled in the aluminium sample holder. All measurements were averaged over 75 scans with an overall duration of 15 minutes approximately per measurement.

For temperature dependent scans, a home built heater was used. The heater was a disc sandwiched between two blocks of metals and coupled to the Aluminium block. The sensor was placed close to the aluminium block and was about 5 mm away from the sample end. Temperature calibration showed that the temperature at the sample end could vary by ± 5° C from the set temperature. However a suitable higher temperature was chosen so that even after the corrections, the sample temperature was close to the required temperature. 15 minutes waiting time was given for the sample to equilibrate and then the scans were made.

Chapter 4

Results & Analysis

4.1 Analysis of internal structure of lamellar P(S-b-ODMA) copolymers

4.1.1 Structural analysis of the sample LAM20

4.1.1.1 Small angle and Wide Angle X-ray scattering data for Shear Oriented LAM20 Samples

The results of the various small angle and wide angle X-ray scattering experiments performed in order to evaluate the internal structure of the PODMA domains in the block copolymer LAM20 are compiled in this section.To give an overview, integrated intensities from SAXS and WAXS measurements on sample LAM20 are given in fig 4.1.

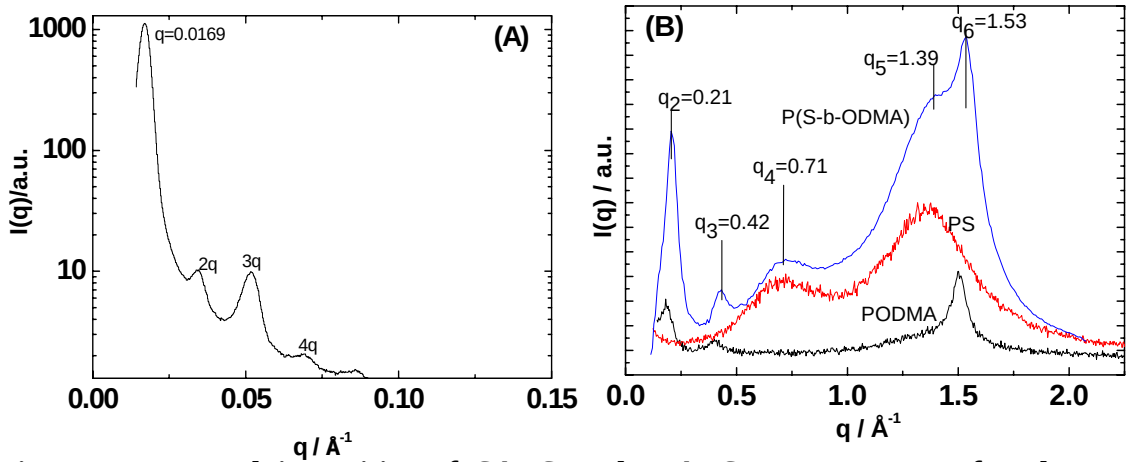

Fig 4.1 Integrated intensities of SAXS and WAXS measurements for the sample LAM20. WAXS data for the homopolymers are shown for comparison. The curves in (B) are vertically shifted.

SAXS measurements showed peaks at q=0.0169 Å $^{-1}$ and at integral multiples of q. The first order peak according to the Bragg equation d=2π/q corresponds to a spacing of d=371Å. The lower intensity of even order peaks is characteristic of this system in the semi-crystalline state. Previous studies[57] have shown this effect disappears when amorphous samples are measured at temperatures above the melting temperature of PODMA**.** It is known that the disappearance of even order peaks is a typical feature of symmetric block copolymer due to a convolution of structure factor and form factor.

WAXS measurements (fig4.1 (B)) show peaks at q_2=0.21, q_3 = 0.42, q_4 = 0.71, q_5 = 1.39, q_6 = 1.53 Å^{-1}. The peak q_2, nomenclatured 'Pre-peak' arises from the semi-crystalline

lamellae formed by the alternating nanophase separated main chains and side chains of PODMA with a spacing of d=29.9 Å. The peak at $q_3=2q_2$ is the higher order belonging to the peak at q_2 and indicates lamellar packing of main and side chains in PODMA domains. The peak at q_4 originates from the PS phase and the amorphous halo with a maximum at q_5 includes contributions from the PS phase and amorphous PODMA. The peak at q_6 (d=4.1Å) corresponds to hexagonally packed PODMA side chains in the crystalline state.

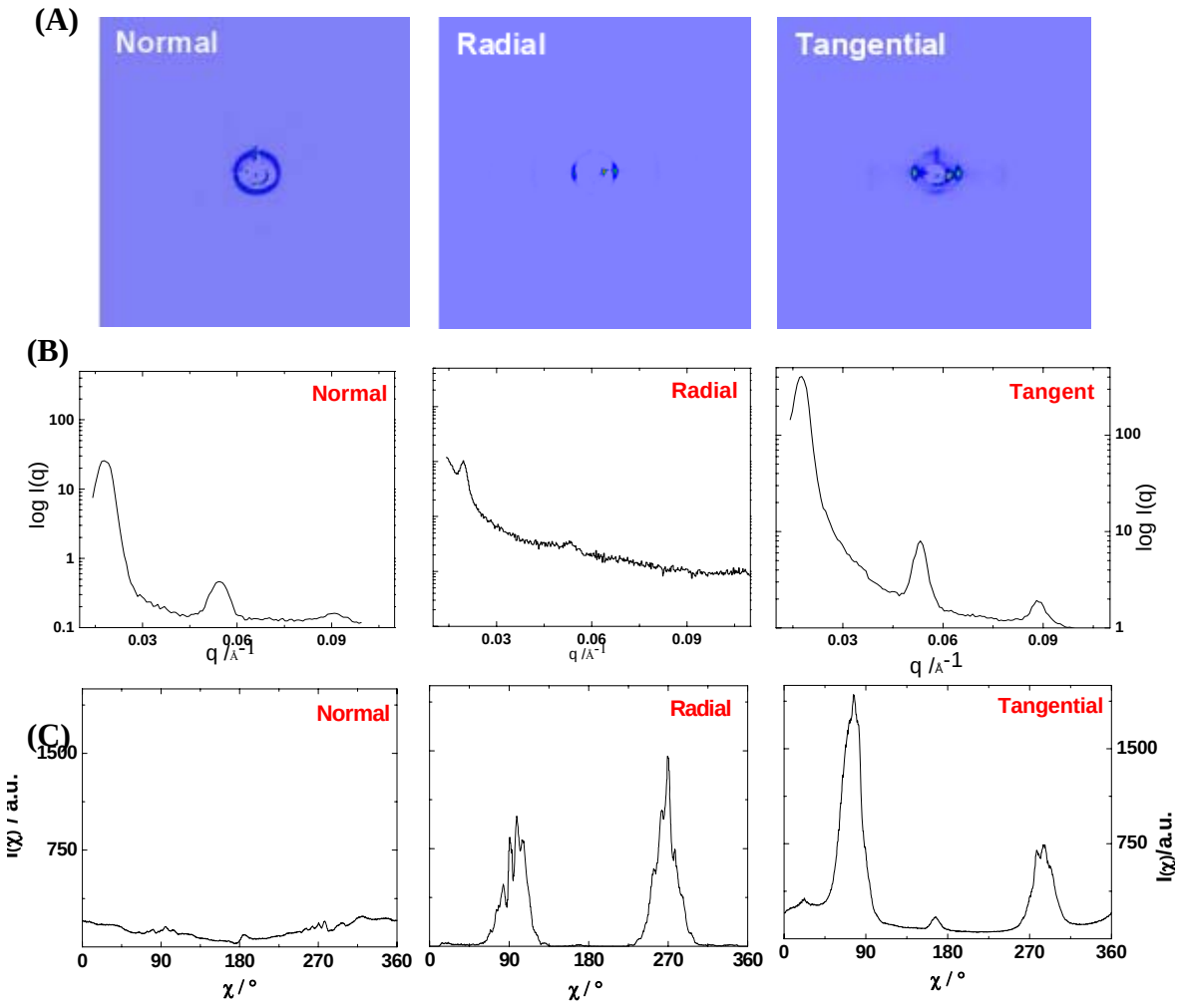

Figure 4.2. (A) Three orthogonal views of 2D-SAXS figures for the sample LAM20 sheared according to program Rheo III. (B) Integrated intensity as a function of q. (C) Radially integrated intensity of first order peak ($0.014<q_1<0.021$ Å^{-1}) as a function of azimuthal angle.

The 2D-SAXS patterns of an oriented sample LAM20 sheared according to the program Rheo III (see table 3) along with the q-dependence of the scattering intensity are given in fig 4.2. The azimuthal angle dependence of scattering intensity that is procured by integrating upon scattering vectors in the range 0.014<q<0.021 is shown in fig.4.2 (C).

It is clear from the 2D-SAXS pictures and the azimuthal dependence that the radial and tangential view show anisotropic contributions while the normal view is isotropic. In the tangential view, there is a small component in the vertical direction (at χ~15 & 170°) but the intensity of these peaks are very less compared to the other peaks. Moreover, it is not clear whether or not these are primary beam contributions. Thus we conclude that the lamellae are basically oriented in parallel orientation.

Data from 2D-WAXS measurements for the same sample are presented in fig 4.3.

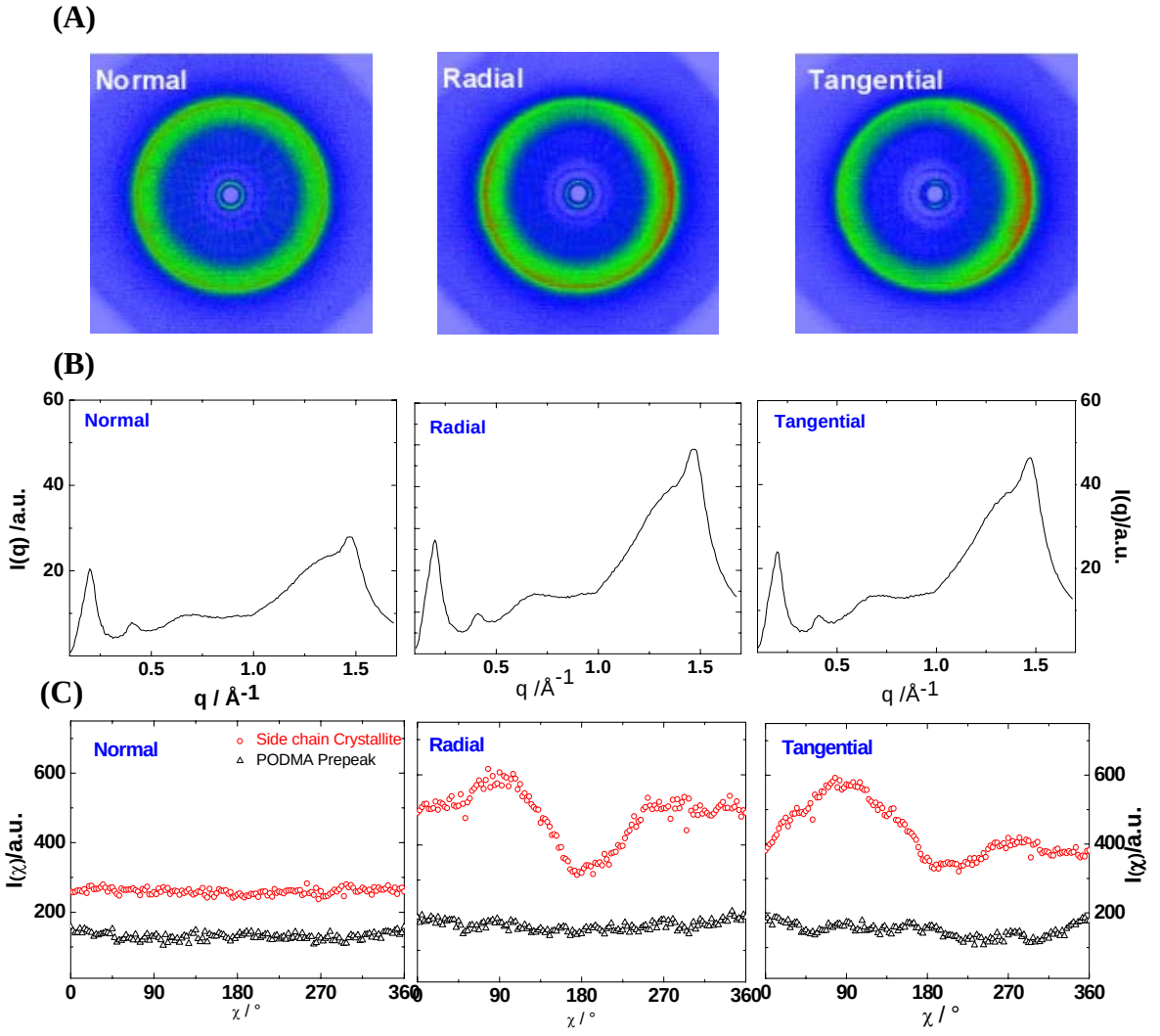

Figure 4.3. (A) Three orthogonal views of 2D-WAXS figures for LAM20. (B) Integrated intensity as a function of q. (C) Azimuthal angle dependence of intensity of contributions from pre-peak ($0.127<q_2<0.255$ Å^{-1}) and the side chain crystallites ($1.45<q_6<1.6$ Å^{-1}) .

All typical peaks of semi-crystalline P(S-b-ODMA) are observed and basically there are no changes in the peak position. Radial integration was done in the range $0.13<q_2<0.26$ Å^{-1} to include PODMA pre-peak contributions and in the range $1.45<q_6<1.60$ Å^{-1} to include

the crystalline side chains contributions. It is clearly seen that there is not much orientation of the PODMA pre-peak in all three views. In the tangential view, there is an asymmetry at large q values, typically for q>1 $Å^{-1}$, that can be seen by comparing the sections χ=0-180° and χ=180-360°. This is a technical problem that appears in all measurements made with sheared samples, which makes it difficult to derive any serious conclusions from large q values in the figure. The different path lengths travelled by the X-ray beam through the sample could be one reason for this problem.

Despite this problem of asymmetric contributions, it should be mentioned that some anisotropy exists in the contributions coming from the side chain crystallites in the tangential and radial views indicated by the peaks at χ=90° and 270°. The peak at q_6 in the normal view, however, is quite isotropic. Note that in this direction the problem with asymmetry disappears.

The above mentioned situation could be considered as a typical case of shear oriented LAM20 sample. In all the programs that we have used after Rheo III(cf. Table 3), clear orientation of block copolymer lamellae was observed, but the PODMA pre-peak, that corresponds to the period of the lamellae formed due to alternating main and side chains remained unoriented, and hence the results did not yield much information about the internal structure of the PODMA domains. This indicates that oriented PODMA lamellae are not a priori connected with the orientation of the structural elements of the PODMA domains. This is partly unexpected since nanophase separation and side chain crystallization still exist in these systems with relatively short PODMA main chains. Further details will be discussed in Chapter 5.

4.1.1.2 SAXS and WAXS data for Extruded LAM20 samples.

Since we did not observe significant orientation of the main chains in shear oriented LAM20 samples we prepared fibers by ‘Extrusion’ of microphase separated samples to orient the lamellae. The SAXS figure of an extruded sample is given in figure 4.4.

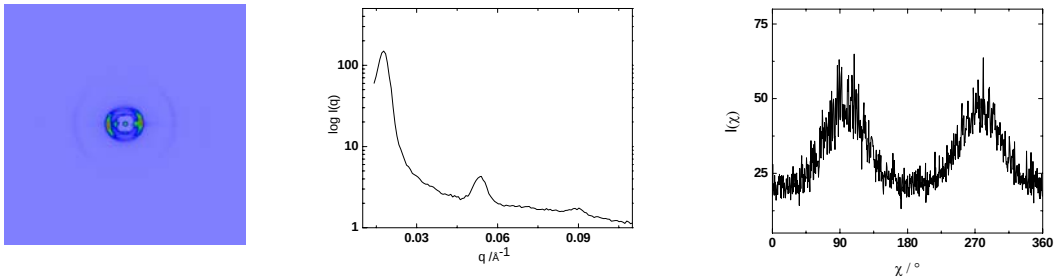

Figure. 4.4 2D-SAXS figure for an extrudate(A). Integrated intensity as a function of q. (B) and as a function of χ(integrated in the range: 0.014<q_1<0.021 $Å^{-1}$) (C).

The samples show orientation with the lamellar normal oriented perpendicular to the fibre axis which was the case for all extruded samples.

2D-WAXS patterns for some of the fibers were obtained. These are given in fig. 4.5.

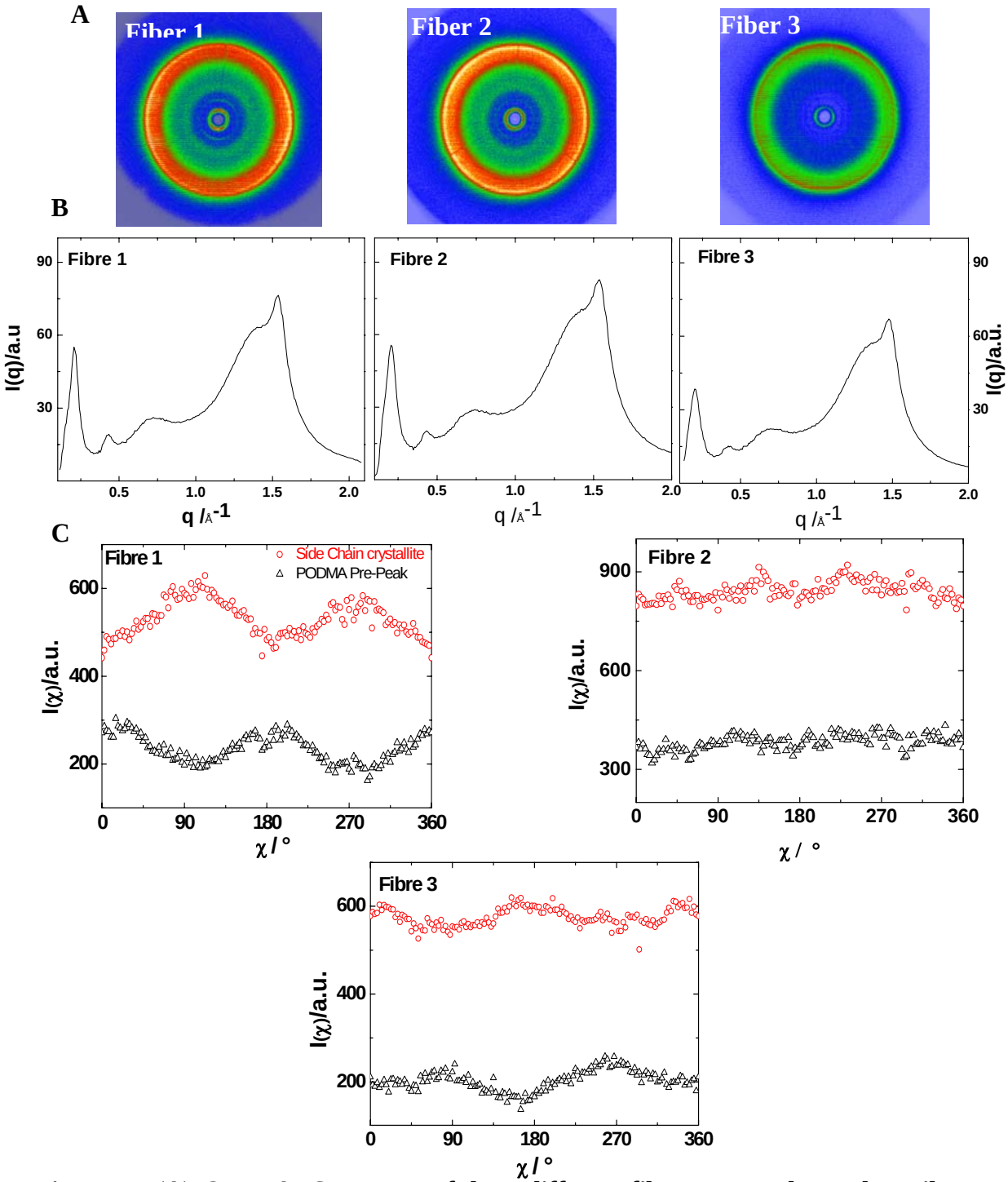

Figure 4.5 (A): 2D-WAXS patterns of three different fibers nomenclatured as Fibers 1, 2 and 3. Clearly seen are the different cases of orientation of PODMA Pre-Peak. (B) Integrated intensity as a function of q and (C) radially integrated intensities for the 2D figures in the range ($0.127<q_2<0.255$ Å^{-1}) for the pre-peak and ($1.45<q_6<1.6$ Å^{-1}) for the side chain crystallites.

Given that, the fiber axis was always vertical and perpendicular to the beam in all the measurements and no intentional changes were made in the preparation conditions, three completely different cases of orientations of the PODMA pre-peak in the WAXS measurements were observed (fig 4.5). In case, of fiber 1, the nanophase separated lamellae is oriented perpendicular to fibre axis, while in case of fiber 3, it is oriented parallel to the fibre axis. Interestingly, in case of fibre 2, it is not oriented seen from the isotropic contributions of the pre-peak.

Assuming that the position of the fiber with respect to the beam during measurements in SAXS and WAXS to be the same (vertical) with an error margin of (± 5°). The two measurements i.e. the SAXS and the WAXS measurements for the fibre 1 are integrated together and presented in 4.6 as one figure showing azimuthal angle dependence of intensity.

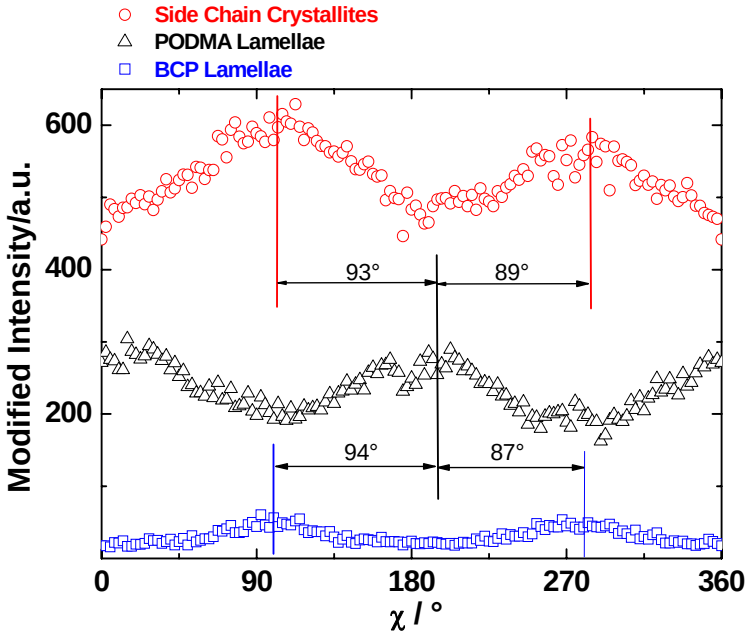

Figure 4.6. Azimuthal dependence of intensity of the three structural features namely copolymer lamellae ($0.014<q_1<0.021$) from SAXS, and PODMA pre-peak ($0.127<q_2<0.255$ Å^{-1}) and side chain crystallites ($1.45<q_6<1.6$ Å^{-1}) from WAXS.

Clearly seen is the orientation between the various structural elements. The pre-peak arising from the nanophase separated main and side chains of PODMA can be perceived to be perpendicular to the block copolymer lamellae and the side chains, well within the error range of the experiment. That is the normal to the nanophase separated lamellae and the side chain crystallites are oriented parallel to the interface between PS and PODMA lamellae. These results thus include the orientation details in the block copolymer.

To see the effect of side chain crystallization on orientation, we made simultaneous measurements while cooling the fiber 1 to 10°C from room temperature, then annealing at 60°C for one hour, and cooling back the sample to 10°C for 75 minutes. The results of the experiment are given below in fig 4.7.

(A)

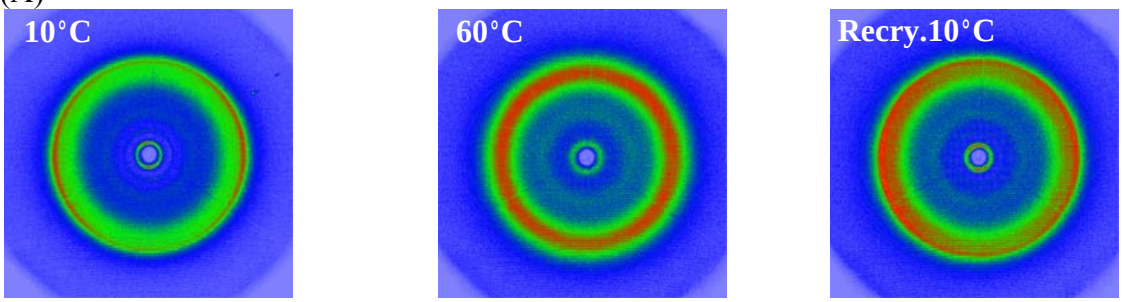

(B)

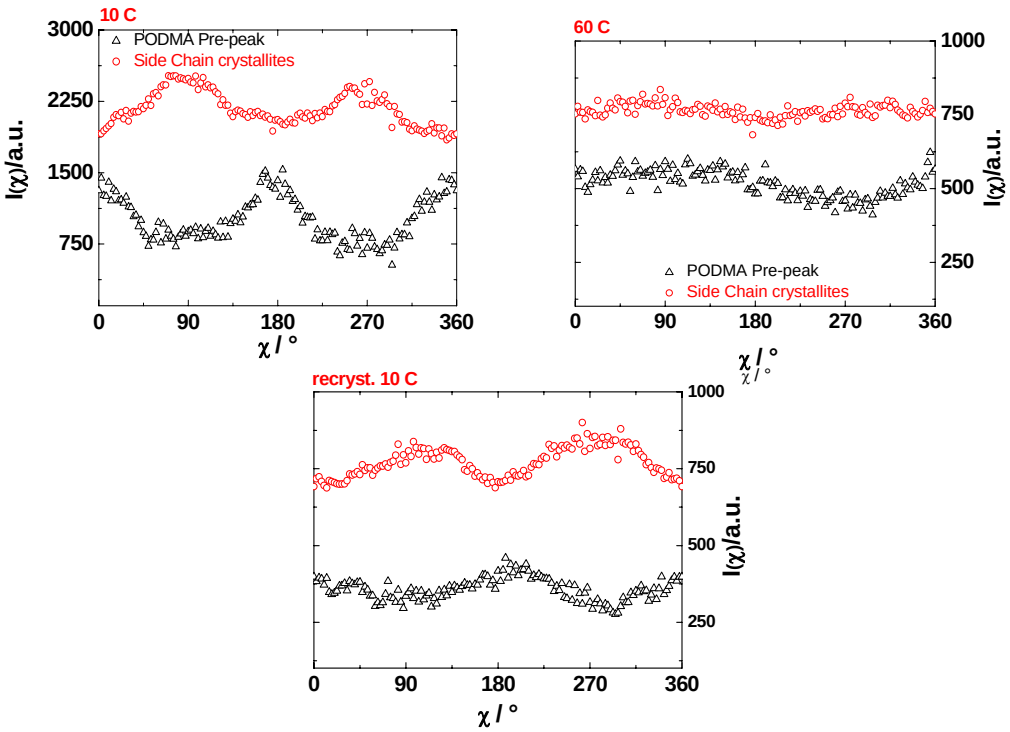

Figure 4.7. (A) **WAXS patterns of measurements done at 10°C, then heated to the molten state (at 60°C) and once again cooled to 10°C. (B) Azimuthal angle dependence of PODMA pre-peak intensity ($0.127<q_2<0.255$ Å^{-1}) and crystalline side chain intensity($1.45<q_6<1.6$ Å^{-1}) .**

Initially the PODMA main chains are obviously oriented as indicated by the anisotropic pre-peak contributions. The contributions become isotropic on melting and once again anisotropic on cooling. Comparing the pre-peak belonging to the PODMA main chain-main chain distance at 10° C, before and after melting, we see that the intensity has decreased and the peak width has increased.

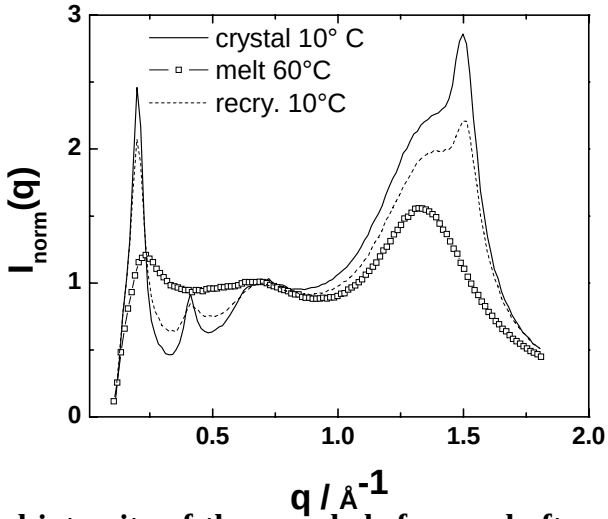

Figure 4.8. Integrated intensity of the sample before and after melting normalized to the peak at q = 0.71Å^{-1}.

For comparison, the intensities of each curve is normalised to the intensity of the peak at q_4=0.71Å^{-1}, that is confirmed to be originating from Polystyrene. Comparing the peak intensity of the side chains crystallites (see fig.4.8), given by the peak at q_6~1.5**Å^{-1}**, before melting and after cooling from the melt at 10°C, we see a marked decrease after melting. This indicates that the degree of crystallinity after melting is significantly smaller than before. Note that it has been shown that for PODMA homopolymers that the higher order peak q_3 occurs only after long periods of crystallization and large degrees of crystallinity (D_C^{PODMA} > 25%)[39]. Seemingly this second order peak develops faster in block copolymers where the PODMA are fixed in PS-PODMA interfaces. In order to come to a final conclusion about the effect of crystallization on orientation, more experiments have to be conducted on samples with varying degrees of crystallization.

4.1.1.3 Scanning Electron Microscopy of LAM20

In order to get support for the polymer morphology obtained from SAXS data and to learn more about the orientation of the block copolymer lamellae, scanning electron microscopy experiments were performed. The scanning electron micrographs of LAM20, one sheared (according to progIII as in table 3) and another extruded are given in fig. 4.9. Scans were done on the extruded sample end-on that is along the fiber axis and on the sheared sample in the plane defined by the radial or tangential vectors as normal.

The micrographs confirm the lamellar nature of the block copolymer domains. The average of the measured domain length from the micrographs was found to be

37.2 nm. This value corresponds well to the periodicity determined from SAXS experiments (d=37 nm).

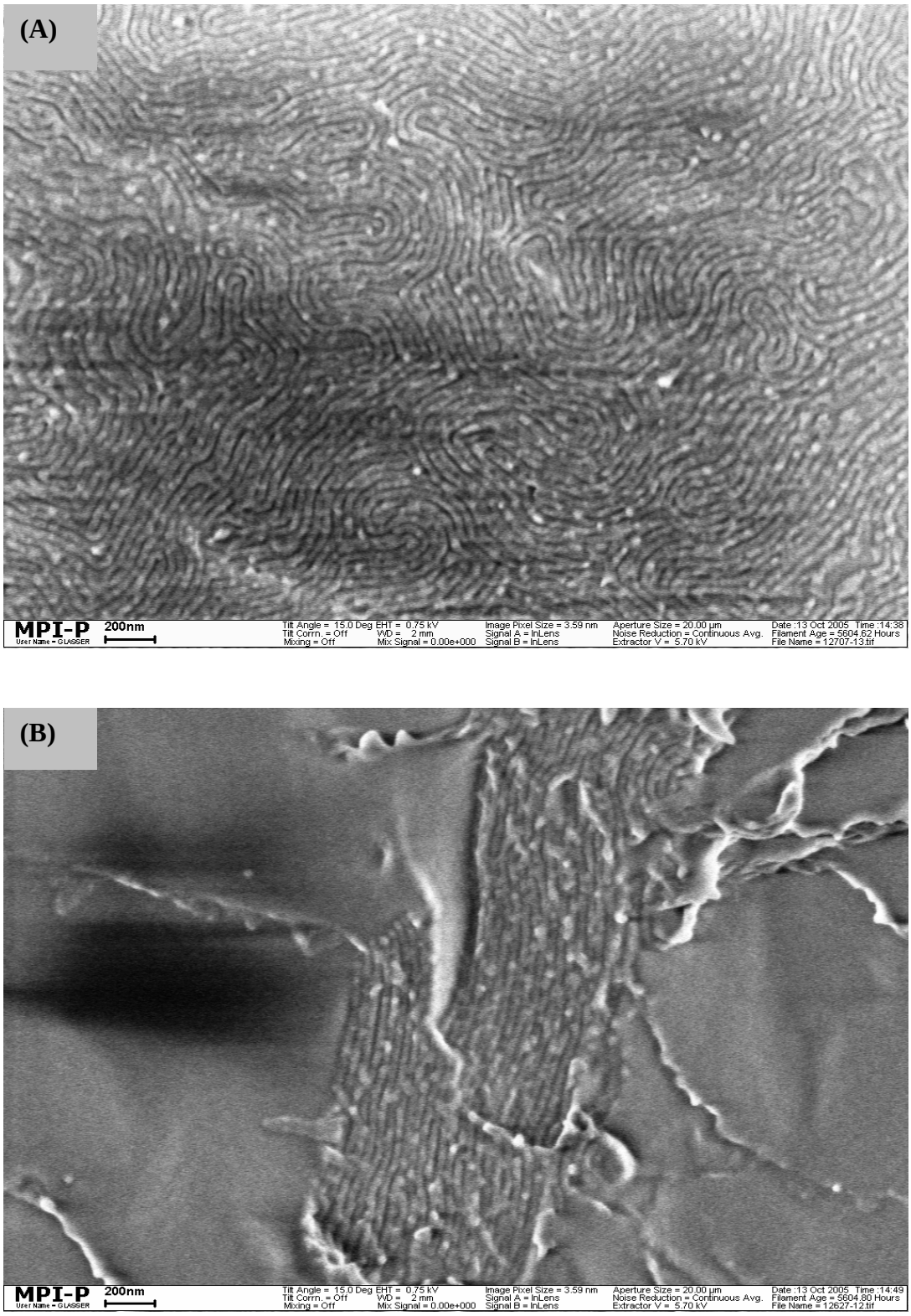

Figure 4.9 Scanning electron Micrographs showing surface morphology of (A) an Extruded LAM20 sample and (B) shear oriented LAM20

In the case of sheared samples, we were able to view the lamellae edge-on as well as flat-on, while in the case of extruded samples, only lamellae with edge-on were visible. This clearly fits with the scattering pictures showing that in case of extruded samples most of the lamellae have a normal which is perpendicular to the fiber axis and distributed radially. The sample is basically one dimensionally oriented in this case.

4.1.1.4 SAXS and WAXS data for Shear Oriented LAM10:

In order to see if the same situation also prevails in other samples we made measurements on the sample LAM10. Lam10 differs from the previously examined LAM20 in terms of block length due to which the domains sizes becomes smaller. Further information about the microstructure can be seen in table 3.2. Representative scattering curves from SAXS and WAXS measurements for the Sample LAM10 are given in fig 4.10. In general, the scattering curves are quite similar to that of the sample Lam20 shown in fig.4.1.

The lamellar spacing is the major difference between the two samples LAM10 and LAM20. The first order peak in the SAXS measurements, corresponds to a block copolymer lamellae spacing of d=216 Å for the sample LAM10. This means that the thickness of the PODMA lamellae in LAM10 is roughly only half of that for the sample LAM20.

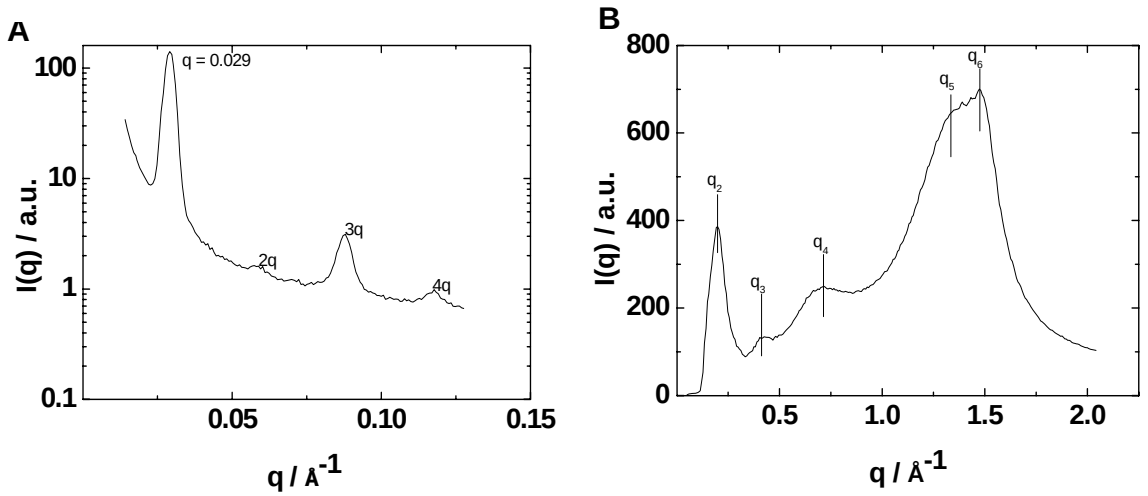

Figure 4.10. Integrated intensities of (A) SAXS and (B) WAXS measurements for the sample LAM10.

The peaks in the WAXS range (fig4.10.(B)) and other phenomenon like the lower intensity of even order peaks of the block copolymer lamellae in the semi-crystalline state seem to be common to both the samples. The occurrence of the peak at q_6 and the small intensity of the odd orders belonging to the block copolymer lamellae indicate that the sample is crystalline. All other peaks can be interpreted as discussed in section 4.1.

LAM10 sample was sheared according to the shear program Rheo I (Table 3). The three measured orthogonal views from SAXS and WAXS measurements are given in fig.4.10.

From the 2D-SAXS measurements, we see that the block copolymer lamellae (fig. 4.10) contribute anisotropically in the tangential and the radial view and an isotropic pattern is observed in the normal view, similar to the sample Lam20. This shows that the sample is highly oriented in parallel direction as discussed in section 2.2 (see fig.2.5)

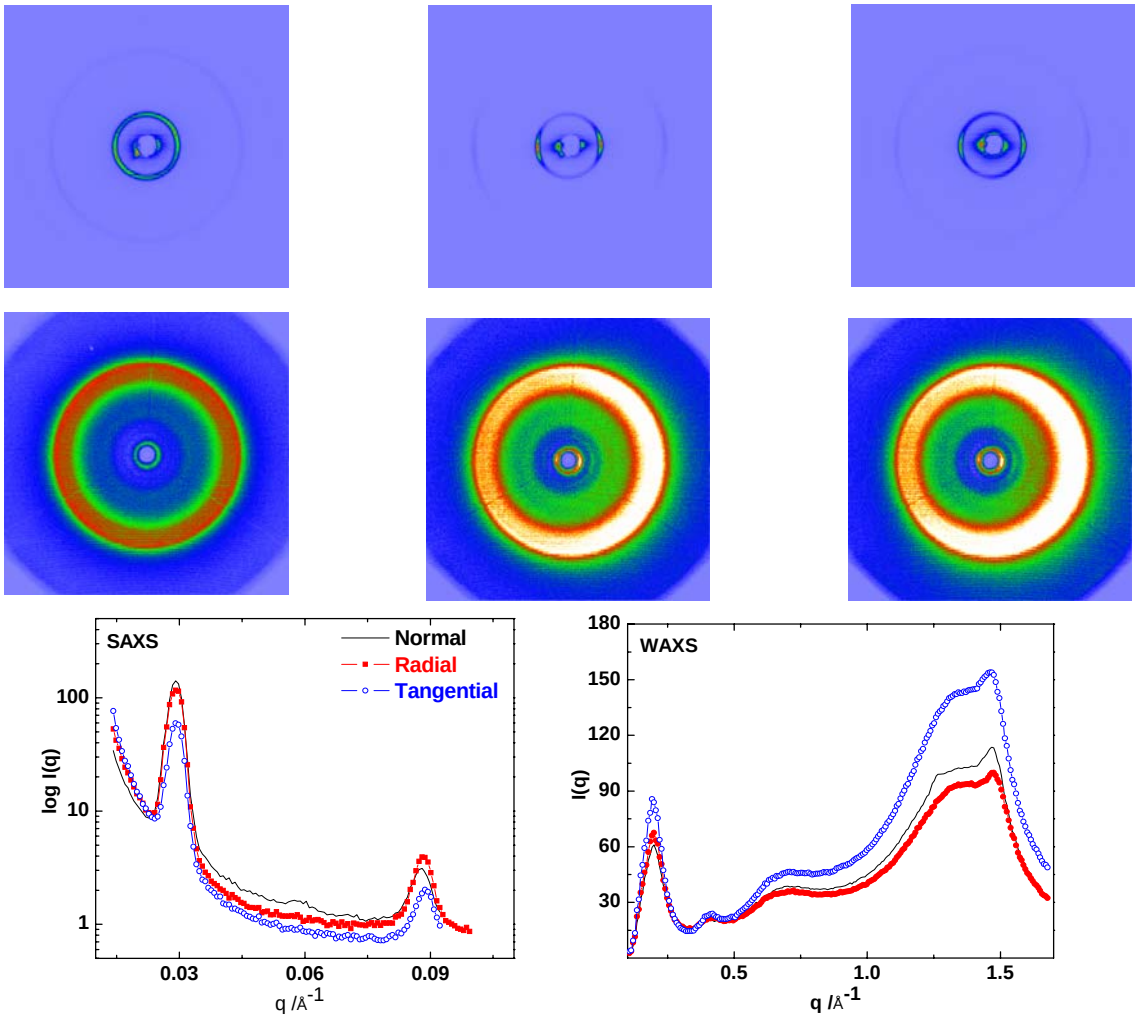

Figure 4.11. TOP: (left to right) Normal, radial and tangential views of the 2D-SAXS measurements for the sample LAM10. MIDDLE: 2D-WAXS data obtained under identical conditions. BOTTOM: The q-dependence of intensity obtained from the 2D-SAXS and 2D- WAXS measurements shown above.

As seen from 2D-SAXS data, the block copolymer lamellae seem to be highly oriented (fig. 4.12.A). The information from WAXS range is given in two separate plots showing the contributions from PODMA pre-peak (fig. 4.12 B) and the side chains (fig. 4.12 C) separately. The PODMA pre-peak is seen to be oriented to some extent in the radial and

tangential views; while the problem of asymmetry dominates in the q-range where the side chain crystallites contributes. Thus nothing can be said about a possible orientation of the side chain in this case as well.

In order to learn more about the orientation, SAXS and WAXS data have been integrated radially in selected q-range. The results are shown in fig.4.12.

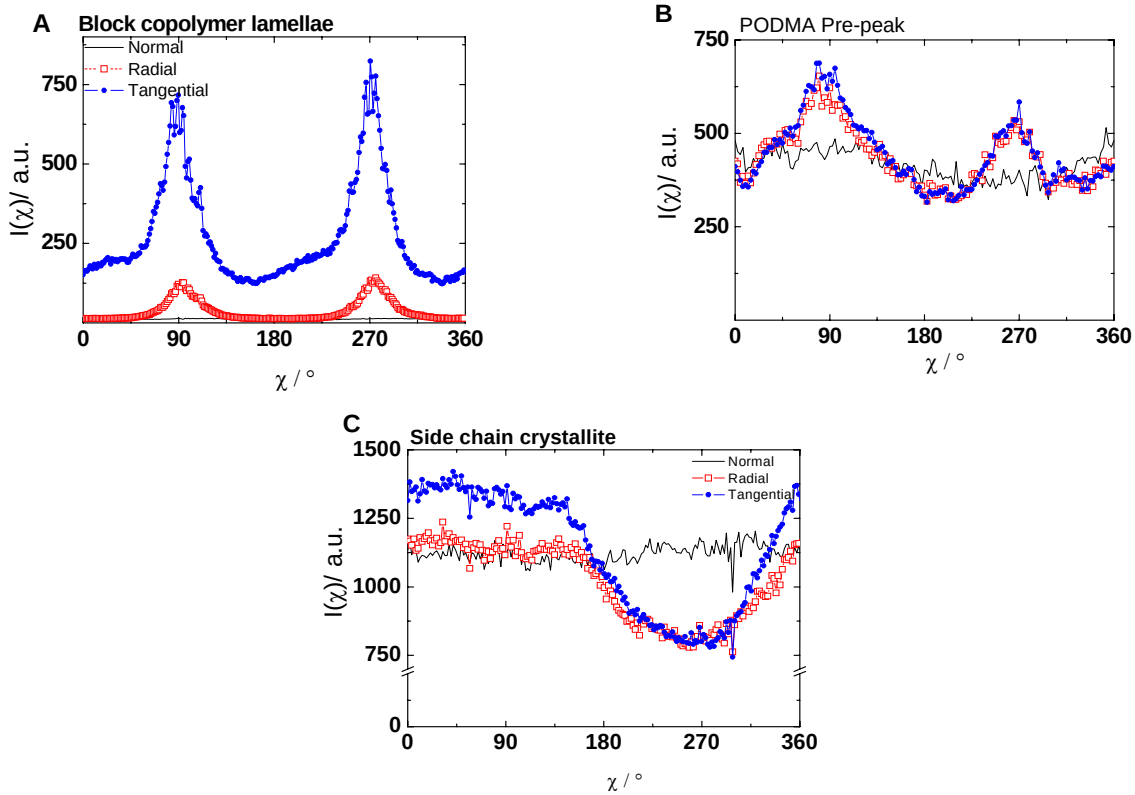

Figure 4.12. Contributions in the three orthogonal views from (A) block copolymer lamellae ($0.024<q_1<0.034$ Å^{-1}), (B) PODMA pre-peak ($0.127<q_2<0.255$ Å^{-1}) and (C) the Side Chain crystallites ($1.45<q_6<1.6$ Å^{-1}).

The interesting and unexpected feature though is the relation between the orientation of block copolymer lamellae and PODMA main chains. We see that they are oriented in the same direction unlike in the case of LAM20. Peaks appear for block copolymer lamellae at (χ ~90° & 270°) and for PODMA pre-peak at the same angles (χ ~90° & 270°) against the expected orthogonal tilting. However, one should mention that the anisotropy in case of the pre-peak is relatively weak and strong isotropic contributions occur. Moreover, there are indications of bimodal orientation.

To confirm this effect, we made measurements in another set-up in University of Halle where the q-range of the equipment (sample-detector distance) was suitable to view peaks corresponding to the block copolymer lamellae and the PODMA pre-peak contributions simultaneously. The integrated scattering intensities of these measurements

show that the q range of the measurement lies well in the above mentioned regime (see fig.4.13).

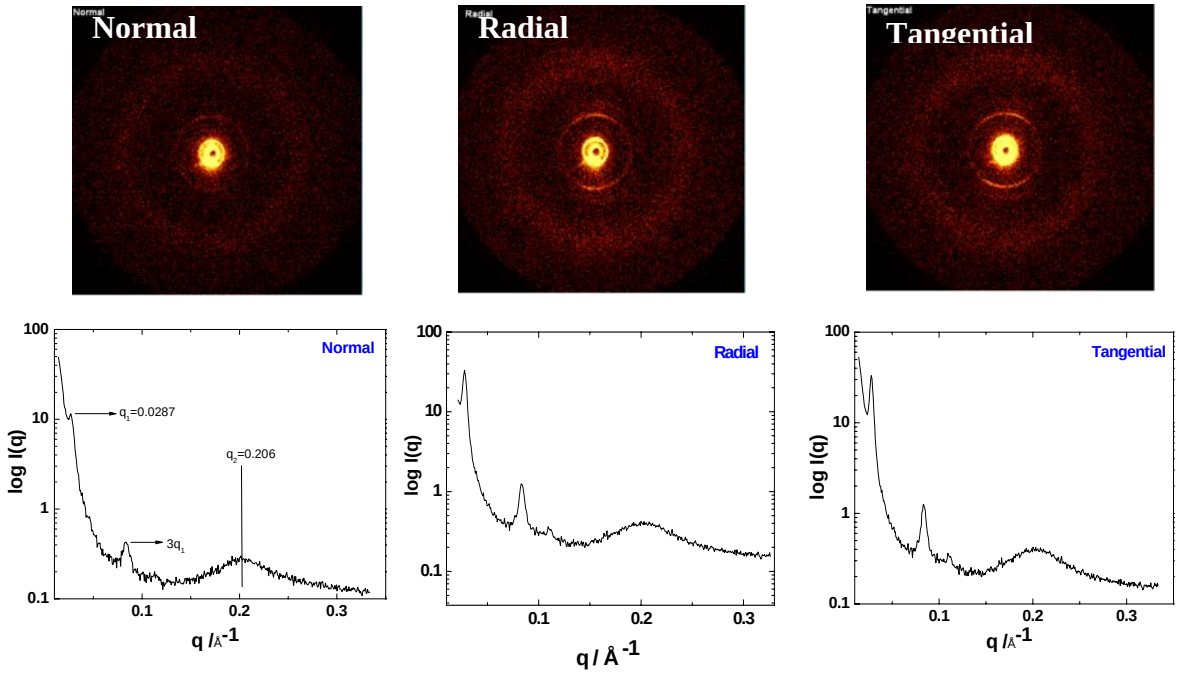

Figure 4.13 Normal (left), radial (middle) and tangential (right) views of the measurements from the setup in Halle along with integrated intensity of the views. The first and the third order lamellar contribution and the pre-peak are labelled together with relevant q-values.

The radially integrated intensities of the measurements made in the three orthogonal views are given in fig. 4.14. Despite the low intensity of the pre-peak it is clear from the measurements that the nanophase separated PODMA lamellae and the block-copolymer lamellae are not oriented perpendicular to each other and seemingly parallel in contrary to the most natural picture for the orientation of the different structural elements.

In the radial and the tangential views, maxima in the pre-peak contributions and the block copolymer lamellae contributions occur basically at the same angle although the pre-peak includes large isotropic contributions. They seem to have an orientation which is parallel with an angle of $\leq 10°$ between them. Note that, contributions from the block copolymer lamellae corresponding to existence of multiple orientations are also seen in these data.

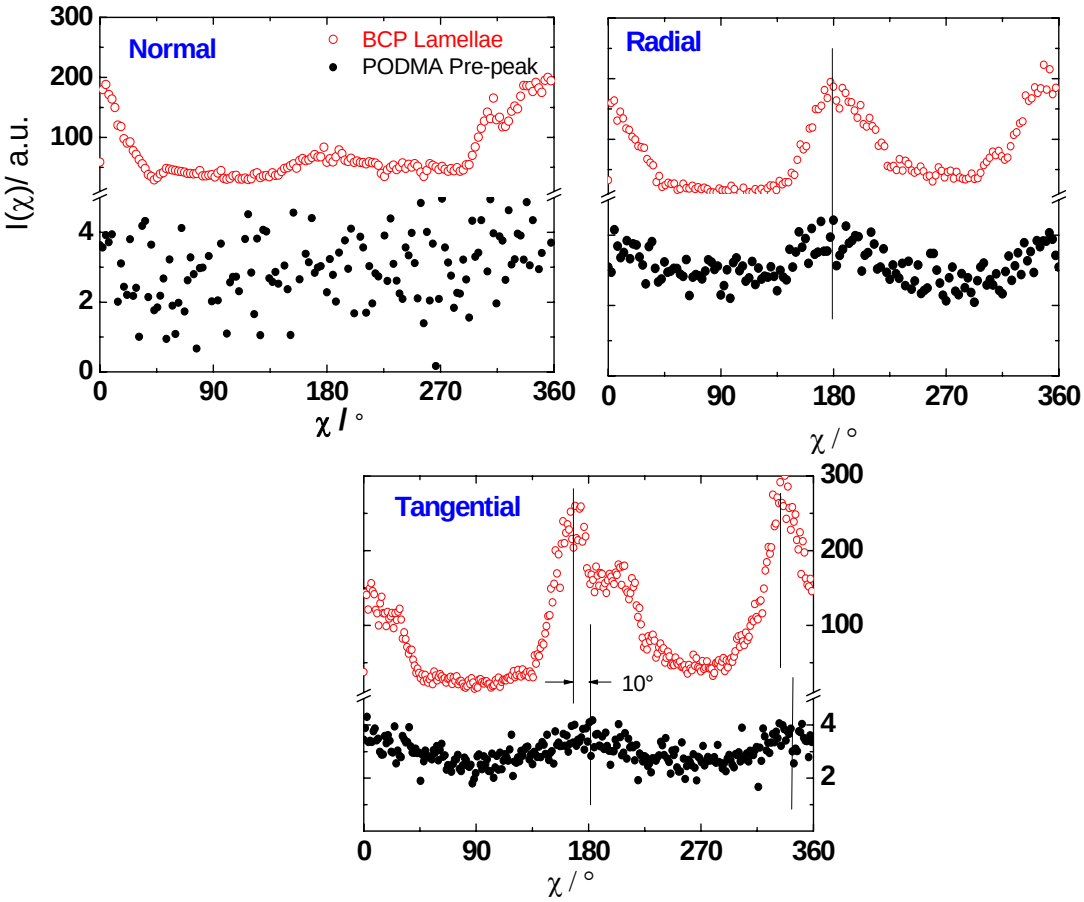

Figure 4.14 The three orthogonal views of the sample LAM10 showing orientation of PODMA pre-peak ($0.172<q<0.27 Å^{-1}$) and block copolymer lamellae ($0.022<q_2<0.036 Å^{-1}$) represented by open closed and open circles respectively.

The SAXS patterns in I(χ) are slightly bimodal in radial as well as in tangential views. That is, parallel orientation may coexist with slightly tilted lamellae. Another unusual feature is the occurrence of a significant distortion in the normal direction. All these facts may indicate that the orientation is not perfect on a macroscopic scale to which extent this may influence the conclusions that can be drawn from the pre-peak contribution concerning the nanophase lamellae orientation. This will be discussed in Chapter 5.

In order to check the influence of degree of crystallinity on the pre-peak anisotropy and the orientation of PODMA main chains, temperature dependent WAXS measurements were made after the sample was stored at -18°C for several hours. Subsequent measurements were made at 10°C. Then the sample annealed at 60°C for 1 hour, then stored at 4°C for 24 hours and once again measured at 10°C. Variation of PODMA pre-peak orientation with temperature in the three orthogonal views is shown in fig.4.15. We can

clearly see that there is no orientation of PODMA lamellae in the normal direction, while there is moderate orientation in radial and good orientation in tangential views respectively at 10°C before melting.

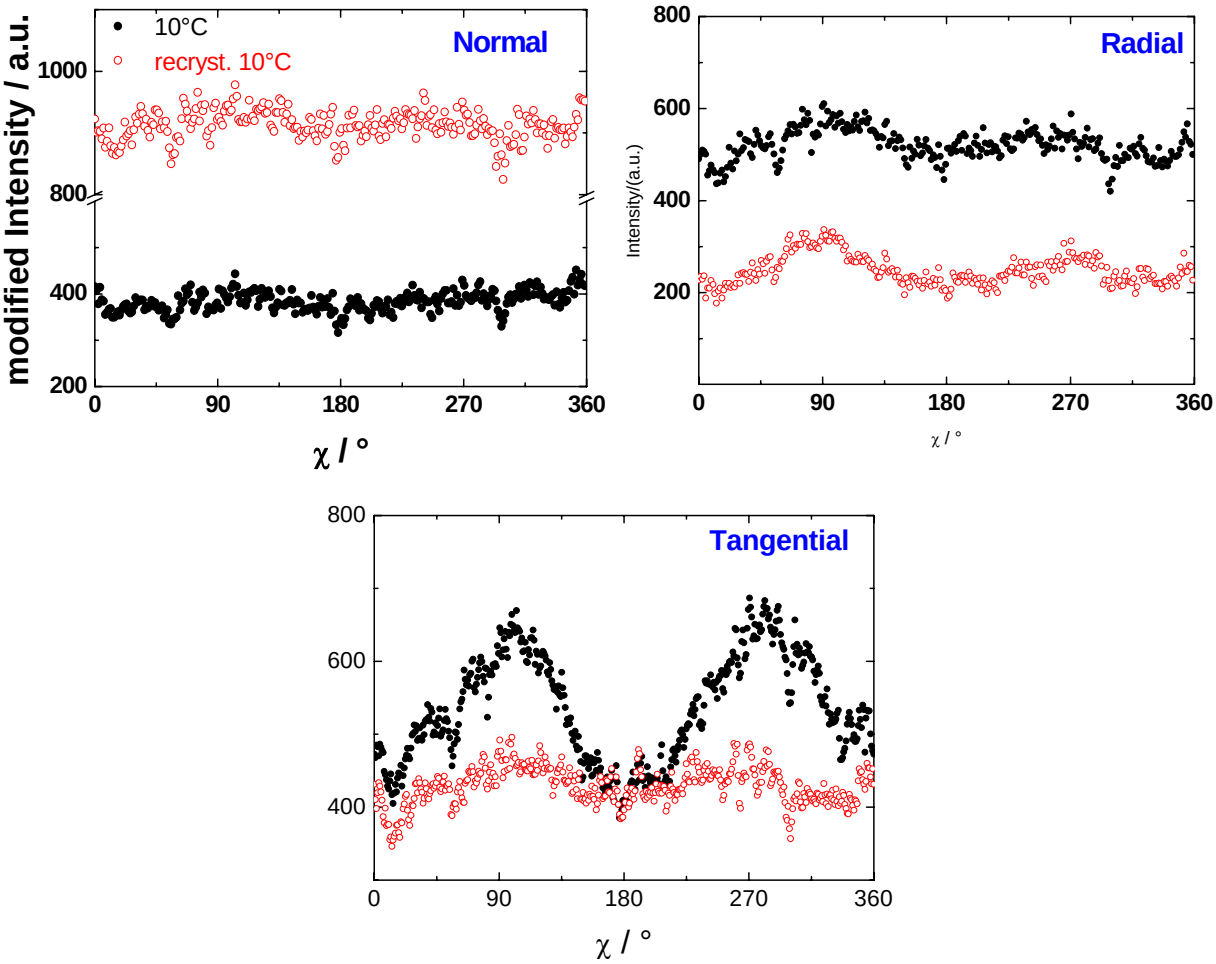

Figure 4.15 Effect of temperature on reorientation of PODMA prepeak (0.172<q<0.27Å^{-1}). Radially integrated Intensity of the three orthogonal views at different temperatures.

The integrated WAXS intensities as a function of q for the three orthogonal views at 10°C before melting, 60°C in the molten state and 10°C after recrystallizing are given in fig.4.16. For comparison, the intensities of each curve is normalised to the intensity of the peak at q_4=0.71Å^{-1}, that is confirmed to be originating from Polystyrene.

There are two temperature dependent effects in these data that require explanation. The first feature is that the pre-peak maximum corresponding to the period of nanophase separated PODMA shifts from 0.19Å^{-1} at 10°C to 0.21Å^{-1} at 60°C, when PODMA is molten, then shifts back upon cooling. This is a known phenomenon[39] and basically related to the degree of crystallinity of PODMA side chains. The trans content in the alkl groups increases during crystallization and the main chain-main chain distance increases.

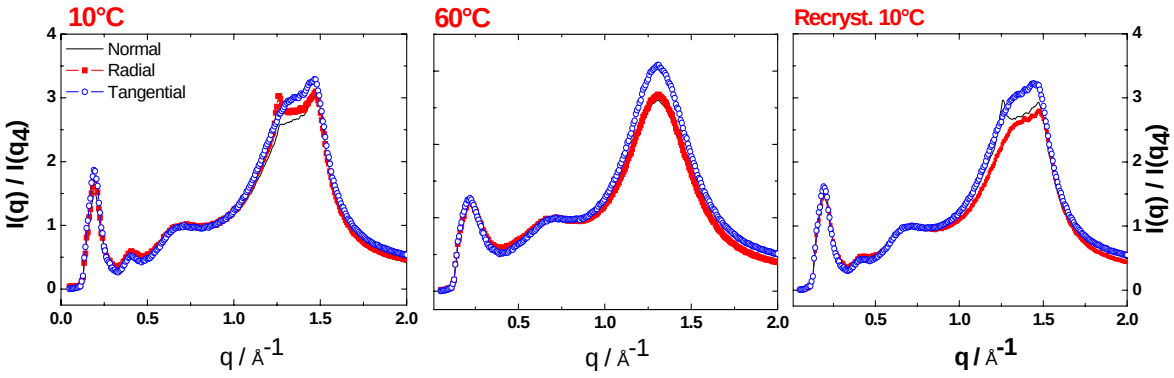

Figure 4.16 Normalised intensities of the three orthogonal views measured after different thermal treatment(see text).

The second, a more remarkable feature is the appearance of an additional peak at q=1.25Å^{-1} in the radial view measured at 10°C before melting, and a clear intense peak at the same position in the normal view at 10°C, after re-cooling. The existence of this peak is supported by the appearance of a strong shoulder in the normal view measured at 10°C before melting. This finding strongly indicates the development of a new crystalline form at temperatures below room temperature. Unfortunately this is a recent and somehow a preliminary observation. Thus this phenomenon could not be studied in detail in this master thesis since the main aim of these experiments was different. However the effects seem to be clear and further experiments should be performed on samples with different thermal history and degrees of crystallisation in order to clarify this topic. A few comments can be found in the chapter 5.

4.2. Studies of crystal thickness studies of side chains in PODMA containing systems

4.2.1 RAMAN Spectroscopic analysis for PODMA containing systems.

Main idea of the RAMAN experiments was to search for LAM modes in order to get more information about the crystal stem length which is not easily available from scattering data in this case. The peaks that correspond to longitudinal acoustic modes are expected to appear at low frequency shifts. From the calorimetric and other data, the number of carbon atoms in the crystallite should be around 5-6 or 8[42], which would correspond then to a LAM vibration in the range from 350 to 650 cm^{-1} according to the knowledge from alkanes[53].

Raman Spectra were obtained for the Block copolymer LAM20, Homopolymer HOMO16 and Polystyrene. Polystyrene spectrum was used to identify individual contributions from PODMA component of the Block copolymer.

The individual spectra are given in fig. 4.17.

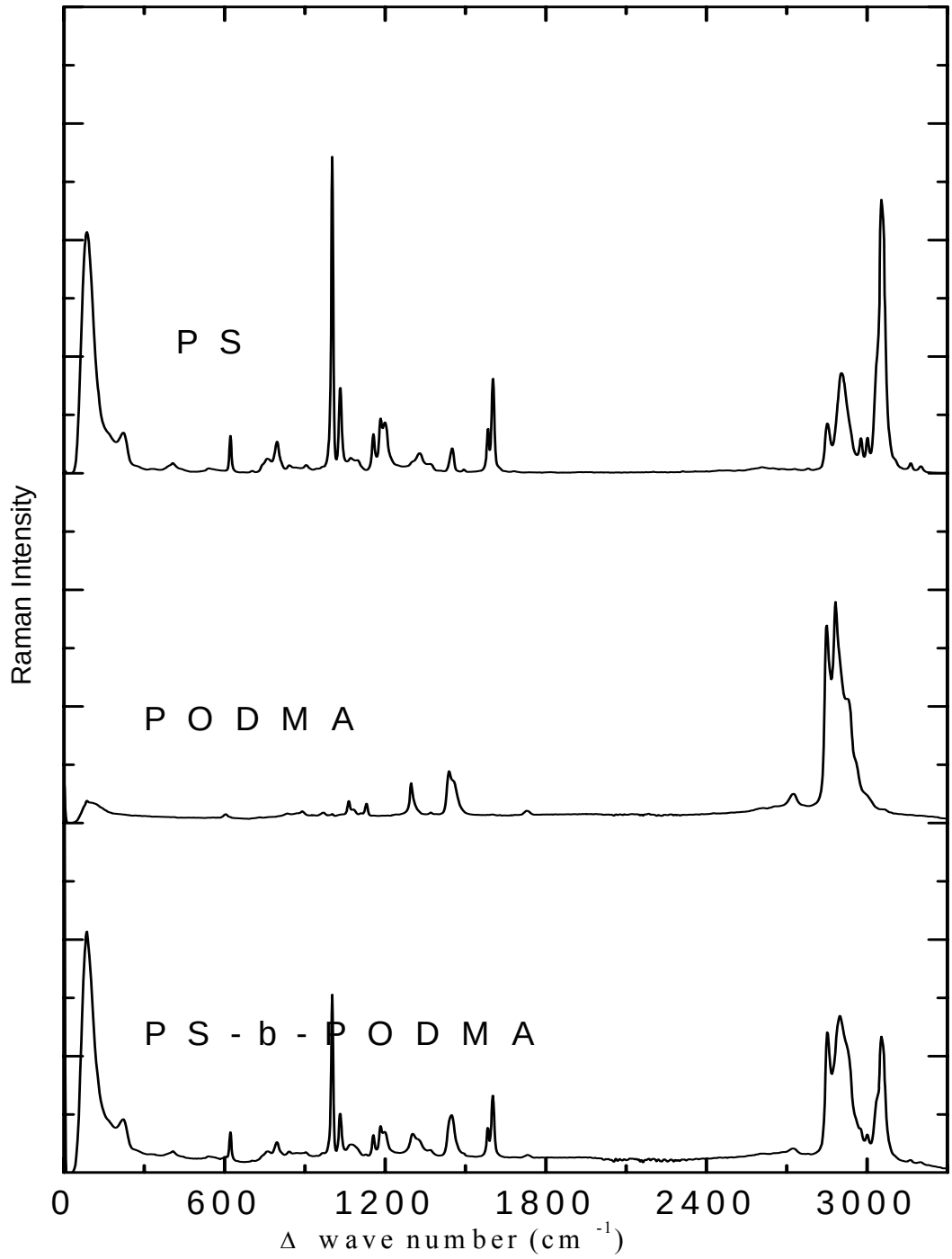

Figure 4.17 Raman spectra of LAM20, block copolymer P(S-b-ODMA),PODMA homopolymer(ODMA 16) and Polystyrene.

Given the fact that crystallinity depends on the thermal history, we expected LAM to occur anywhere from 400 to 700cm^{-1}. There were several peaks in the LAM20 spectrum in this range, but all of them seemed to originate from the Polystyrene fraction as seen in fig

4.18. Nothing can be seen in the relevant wave number range in the spectra for homopolymer.

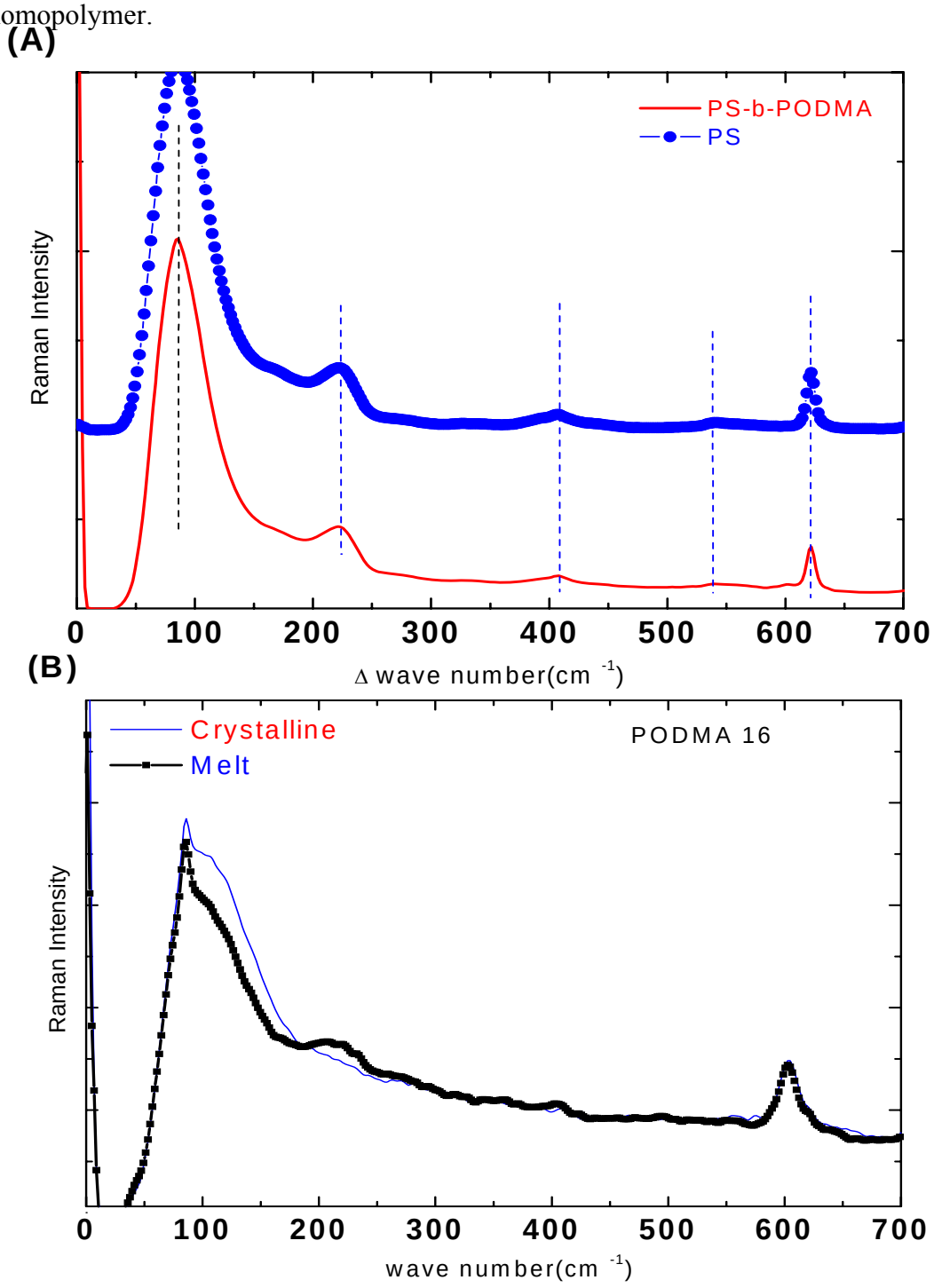

Figure.4.18 (A) Comparison of LAM20 spectra and PS spectra in the LAM range.The curves are vertically shifted. All peaks in LAM20 in this range can be mapped to Polystyrene. (B) Comparison of ODMA spectrum in the melt and in the crystalline states. Note the Peak at 602 cm-1 that appears in both the spectrum.

Another possibility in RAMAN spectra is to get information about trans-gauche content and crystalline packing of the alkyl groups. Amorphous chains that normally occur

in gauche conformation undergo transition to trans conformation during crystallization. The peak at 1080 cm^{-1} has been assigned to gauche conformers in n-alkanes[54]. This feature is also well observed in the case of ODMA16, while it is either clouded by PS contributions or not present at all in the case of LAM20.

In the homopolymer by comparing the intensities of this peak at 1080cm^{-1} in the melt and in the crystalline state, we can find the gauche conformers entering into the crystal.

$$I_{1080}{}^{cryst} / I_{1080}{}^{melt} = 0.05734 / 0.06983 = 0.8211$$

That is, approximately 18% of the gauche conformers have undergone a change into trans conformation. This roughly corresponds to the degree of crystallinity of PODMA at the end of primary crystallization from DSC experiments done with similar thermal treatment.

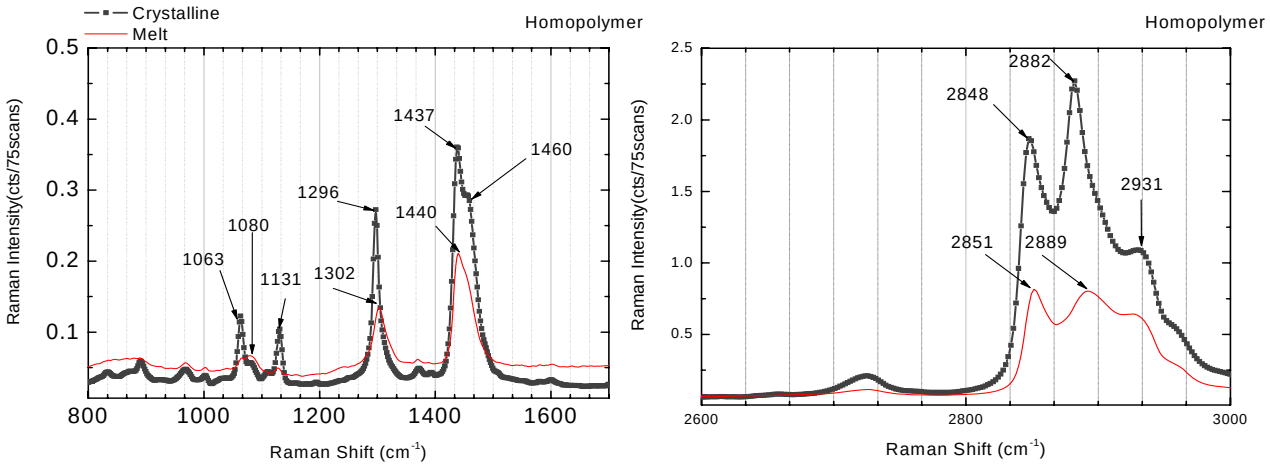

Figure 4.19 PODMA homopolymer spectrum in the melt and in the crystalline state in different ranges.

Another spectral range which includes information about the type of packing is the the range 2800 to 3000cm^{-1}. Bands at 2931, 2851, 2848, 2889 cm^{-1} observed in PE at atmospheric pressure[58] correspond to hexagonal packing. Similar bands are observed for PODMA, while the band at 1417 observed in orthorhombically packed PE is not observed. The spectrum in the range 2800 to 3000cm-1 appears quite similar to the spectrum of hexagonally packed alkanes[54,55].

Chapter 6
Conclusions

The results in this Thesis show that lamellar P(S-ODMA) block copolymers can be oriented by shear or extrusion. Nanophase separation of side chains and main chains as well as side chain crystallization have been observed in the PODMA lamellae in such oriented samples comparable to the situation in bulk PODMA. Although the orientation of the block copolymer is comparable, the orientation of the pre-peak indicating the main chain to main chain distance varies from sample to sample. That makes it difficult to discuss about internal structure of the PODMA domains. In block copolymer samples where the pre-peak is highly anisotropic, the internal structure corresponds to the hypothetical model shown in fig.5.1. Other cases of pre-peak orientation (isotropic pattern or weak orientation parallel to the copolymer interface) have also been observed. These results are not compatible with our simple model(fig.5.1). Otherwise it is hard to imagine that a fraction of PODMA main chains is oriented parallel to the block copolymer interfaces since they are very short Possible origins for this finding have been considered. It is shown that it is hard to get information about the internal structure of the PODMA lamella, if region exist in the sample where block copolymer is misoriented. Indications for that have been observed in SEM pictures.

A new kind of crystalline packing has been observed in a lamellar P(S-b-ODMA) block copolymer (LAM10) after annealing at low temperatures ($T<5^{o}C$), for a few days. This is interesting in the light of findings for other systems containing long ~CH_2 sequences showing hexagonally packed mesophases and additional solid-solid phase transitions. Further experiments are required to explore details of this phenomenon. Similar behaviour has not been observed previously for PODMA homopolymers and other P(S-b-ODMA) copolymer which were cooled fastly to similar temperatures.

.

Raman spectroscopy has been proven to be an effective method to study crystal structure of alkyl side chains in PODMA. The originally expected Longitudinal Acoustic Modes providing information about crystal layer thickness in case of long alkanes have not

been observed in case of semi-crystalline alkyl groups of PODMA. Nevertheless, RAMAN spectroscopy provides helpful information about the change in gauche content in the alkyl groups during crystallization

Chapter 5

Discussions

In the last chapter, it has been shown that microphase separated P(S-b-ODMA) lamella block copolymers can be oriented by the application of shear or by extrusion. All aspects of structure appearing in the PODMA homopolymers as well as unoriented P(S-b-ODMA) block copolymers also appear in these shear oriented samples. Nanophase separation exists within PODMA domains shown by the existence of the peak at q_2 (fig4.1B). The peak at q_3 can be regarded as regular lamellar packing of side and main chains as regarded in PODMA homopolymers. Side chains are able to crystallize as shown by the peak at q_6 in a hexagonal lattice at room temperature. All these observations are applicable for both the samples, LAM10 and Lam20, used in this study. Based on scattering results on unoriented samples, a hypothetical picture for the internal structure of the PODMA domains in the block copolymer system has been suggested which is given in fig.5.1.

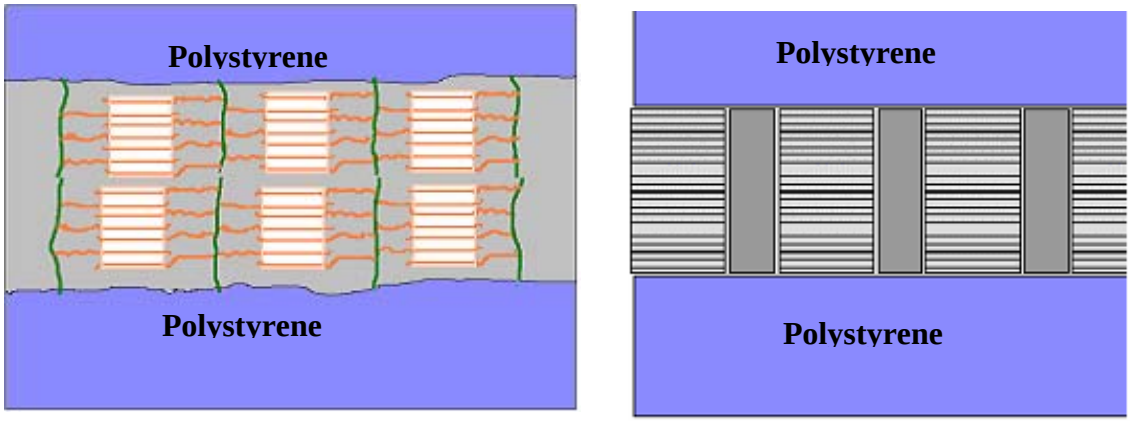

Figure 5.1. Hypothetical pictures showing the internal structure of the PODMA domains in a P(S-b-ODMA) copolymer system (left) and the packing of main chain domains (dark boxes) and alkyl nanodomains (striped boxes).

One of our extruded LAM20 samples (Fibre 1) showing the best orientation of the pre-peaks of all samples confirms to the picture above. The normal to the lamellae formed due to alternating main chains and side chains is oriented perpendicular to the normal of the block copolymer lamellae. The side chains lie perpendicular to the PODMA main chains and parallel to the copolymer interface(fig 4.6). In general, in all cases, where strong pre-

peak orientation is observed, the pre-peak pattern at q_2 is perpendicular to the pattern at q_6 belonging to the side chains. The side chains are oriented perpendicular to the main chains.

However concerning the pre-peak orientation, other cases where the pre-peak is unoriented or oriented parallel to the block copolymer interface also occur. In case of the fibres, the pre-peak orientation varies from sample to sample (see section 4.1.1.2) although the block copolymer lamellae in all fibres are oriented identically having a normal perpendicular to the fibre axis. The pre-peak orientation is sometimes isotropic and in rare cases parallel to the block copolymer lamellae. In case of shear oriented LAM20 samples, inspite of the seemingly well oriented block copolymer lamellae, the pre-peak remains unoriented in most cases. In the case of LAM10, even a weak parallel orientation is indicated. These findings are inconsistent with the hypothetical picture shown in fig.5.1 under the assumption that the peak q_2 indicates main chain-main chain distance in the PODMA domains. The main chains have a length which is not too different from that of the side chains. Thus dominantly parallel orientation of the main chains to the copolymer interface is hard to imagine. Otherwise it is also hard to refute that the peak q_2 does not correspond to the main chain-main chain distance based on scattering data for poly(n-alkyl methacrylates) with different side chain lengths.

The question appears why inspite of block copolymer lamellae orientation, do the pre-peak is isotropic. There can be different effects which will contribute to the isotropization of the pre-peak.

(i) The model in fig 5.1 assumes that the side chains and main chain aggregates into a nanophase separated lamellae within the ODMA domains. In X-ray scattering, if these lamellae are oriented edge-on to the beam, a highly anisotropic pre-peak is obtained. On the other hand, if these lamellae are stacked flat-on, the pre-peak will be isotropic with a small intensity. In principle, the nanophase separated lamellae could be oriented anywhere between these two extremes. That is there is no preferred orientation of the nanophase lamellae, although PODMA lamellae themselves are highly oriented. One can expect differently oriented grains. Within each of these grains the nanophase lamellae are well oriented but the resulting 2D-scattering pattern is an ensemble average of all individual

grains. Thus the pre-peak somehow would resemble a 2D-powder pattern. as shown in figure 5.2A.

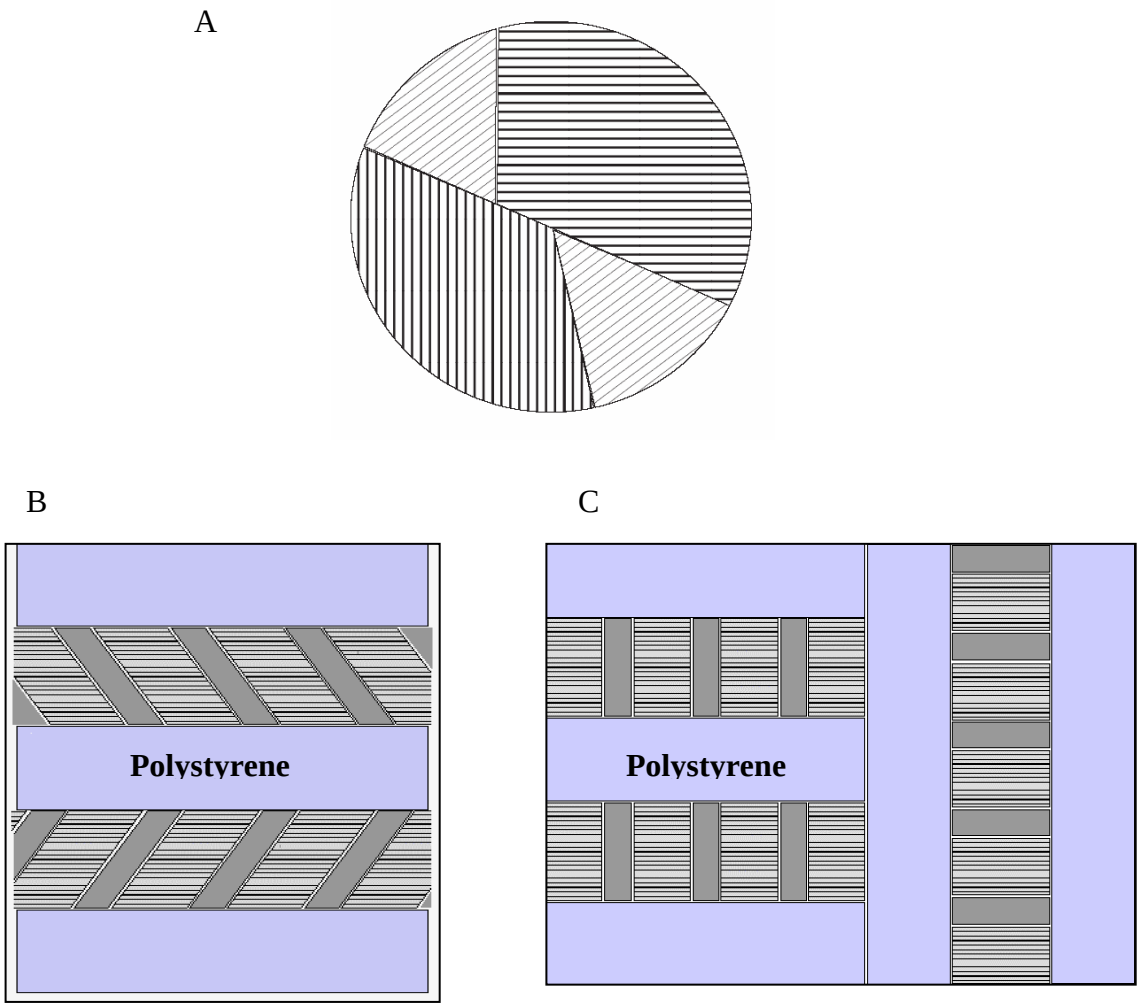

Figure 5.2. (A) Model showing the grain patterns of the nanophase lamellae. (black lines:main chain domains, white region:alkyl nanodomains). (B) Model showing tilted nanophase lamellae. (C) Model showing mis-oriented block copolymer lamellae .

However, in the above considered case, the anisotropy of the pre-peak has to be preserved since the nanophase separated lamellae are assumed to be oriented perpendicular to the block copolymer lamellae. Thus the above model neither explains the isotropy nor other orientation of the nanophase separated lamellae. Only variations in the pre-peak intensity can be explained.

(ii) A second effect that could occur is the tilting of the nanophase separated lamellae with respect to the copolymer interface as shown in fig 5.2B. Such a tilt could explain wide arcs in the pre-peak contributions. The distribution of the tilting angles is directly reflected by the intensity distribution within the arcs. However large tilting angles which are required for an isotropic pre-peak pattern are practically impossible in our systems which have main chains with lengths of 25-50 ODMA units which is not much longer than that of the side chains. It is thus hard to imagine that long main chain segments are oriented parallel to the P(S-ODMA) interface. In summary, both effects discussed above,(i) and (ii), are unable to explain isotropic pre-peaks.

(iii) So far, we have assumed that the block copolymer lamellae are ideally oriented on a macroscopic scale. However, the existence of regions where the copolymer lamellae are oriented differently is not ruled out in real samples. Indeed there are indications of mis-oriented regions from SEM pictures (see fig4.9).Taking into account this problem, the situation becomes more complex. Isotropic pre-peak patterns can be easily explained if the beam hits a region where the lamellae are mis-oriented. This is shown in (fig.5.2 C). Entities that do not contribute to the SAXS signal in an oriented block copolymer still contribute to the pre-peak intensity in WAXS. That is, even those regions where the block copolymer lamellae normal is parallel to the beam, the normal to the nanophase lamellae is not. Hence these regions can contribute to pre-peak isotropy. The effect of mis-oriented regions in the block copolymer lamellae seem to be very critical for studies focusing on pre-peak anisotropy.

To summarize this part, obviously, there are effects which may explain the isotropicity of pre-peak in cases when the block copolymer lamellae is seemingly oriented but not ideally oriented on a macroscopic scale. The experimental situation could be one or a combination of some or all of the above considered effects (i)-(iii) Thus it is hard to draw final conclusions from scattering results on possible non-ideally oriented samples. Further experiments have to be performed on well oriented samples and experimental progress is required to prepare such samples. One approach to produce such samples of high orientation might be annealing for extended periods (few days at 170ºC). Indications are

there from such preliminary experiments that the defects in the orientation heal with extended annealing and result in highly oriented samples.

Another interesting phenomenon in the reported scattering data is the additional peak that has been recently observed in some samples of LAM10 after annealing for long periods at low temperature (T<10°C) (see fig.4.16). This might be an indication for the existence of other crystalline phases in PODMA, a behaviour which is known in other systems containing long CH_2 groups like alkanes or polyethylene. Note that similar effects have not been observed for PODMA homopolymers and the LAM20 samples fastly cooled to comparable temperatures. Further experiments with different time-temperature programs should be performed in order to puzzle out whether this behaviour is specific for the LAM10 sample or depends on the program. Since this effect was observed only recently very limited information is available. One possible explanation for a change of crystalline structure could be the inclusión of bulky methyl group into the side chain crystallite during secondary crystallization that occurs at low temperatures[56] which changes the crystallite packing.

The Raman scattering experiments were originally conducted to learn more about the crystal stem length from LAM modes, which has been observed for several alkanes. However obviously the LAM modes do not occur in PODMA atleast not at the positions, predicted based on literature results for alkanes. However information about crystallite packing can be derived from Raman spectra. The spectral analysis confirms hexagonal packing of the side chains, in agreement with results from X-ray scattering. Moreover, it has been shown that the intensity of the peak at 1080 $cm^{-1}$is changing with crystallization and is indicative of gauche content in the alkyl groups. This shows that RAMAN spectroscopy can contribute helpful information about the structure of alkyl groups in nano-phase separated side chain polymers.

Bibliography

[1]. C.L. Jackson and G.B. McKenna, Chem. Mater. 8 (1996), 2128.

[2]. A. Schreiber, I. Ketelsen and G.H. Findenegg, Phys. Chem. Chem. Phys. 3 (2001), 1185.

[3]. M.V. Massa, K. Dalnoki-Veress and J.A. Forrest, Eur. Phys. J. E 11 (2003), 191.

[4]. G. Reiter and J.U. Sommer, Phys. Rev. Lett. 80 (1998), 3771.

[5]. Ian W. Hamley, "The physics of Block Copolymers", Oxford university Press, Oxford, 1998.

[6]. Y.L. Loo, R.A. Register and A.J. Ryan, Phys. Rev. Lett. 84 (2000), 4120.

[7]. Huang P, Zhu L, Cheng SZD, Ge Q, Quirk RP, Thomas EL, Lotz B, Hsiao BS, Liu LZ, Yeh FJ Macromolecules 34 (2001),6649.

[8]. R.E. Cohen, A. Bellare and M.A. Drzewinski, Macromolecules 27 (1994), 2321.

[9]. L. Zhu, S.Z.D. Cheng, B.H. Calhoun, Q. Ge, R.P. Quirk, E.L. Thomas, B.S. Hsiao, F. Yeh and B. Lotz, Polymer 42 (2001), 5829.

[10]. Greenberg S.A, alfrey.T. J. Am. Chem. Soc.76(1954) 6280.

[11]. G. Duda, A. J. Scouten, T. Arndt, G. Lieser, G. F. Schmidt, C. Bubeck, and G. Wegner, Thin Solid Films 159(1988),221.

[12] Mierzwa M, Floudas G, Stepanek P, Wegner G, Physical Review B 62 (2000), 14012.

[13]. Hempel E, Huth H, Beiner M Thermochimica acta, 403(2003) 105.

[14]. M. Beiner and H. Huth, Nat. Mater. 2 (2003), 595.

[15]. Plate' N.A. , Shibaev V.P., J.Polym.Sci. Macromolecular review., 8(1974),117.

[16]. Flory P.J.(1953) "Priniciples of Polymer Chemistry",Cornell university Press, Ithaca.

[17]. Bates FS, Fredrickson GH, Ann. Rev. Phys. Chem. 41(1990),525.

[18]. Matsen MW, Bates FS, J.Polym.Sci.Polym.Phys.Ed.35(1997) 945.

[19]. Rangarajan P, Register RA, Adamson DH, Fetters Lj, Bras W, Naylor S, Ryan AJ, Macromolecules 28(1995) 1422.

[20]. Nojima, S.; Kato, K.;Yamamoto, S.; Ashida, T. Macromolecules 25(1992), 2237.

[21]. Rangarajan P, Register RA, Fetters LJ. Macromolecules,26(1993),4640.

[22]. Loo YL, Register RA, Ryan AJ, Macromolecules 35 (2002), 2365.
[23]. Quiram DJ, Register RA, Marchand GR, Macromolecules 30 (1997) 4551.
[24]. Quiram DJ, Register RA, Marchand GR Ryan.AJ, Macromolecules 30 (1997),8338.
[25]. Quiram, D. J.; Register, R. A.; Marchand, G. R.; Adamson, D. H., Macromolecules 31(1998), 4891.
[26]. Loo, Y.-L.; Register, R. A.; Adamson, D. H., Macromolecules 33(2000), 8361.
[27]. Loo, Y.-L.; Register, R. A.; Adamson, D. H., J. Polym. Sci., Part B: Polym. Phys. 38(2000) , 2564.
[28]. Lotz, B.; Kovacs, A., J. Polym. Prepr. (Am. Chem. Soc., Div. Polym. Chem.) 10(1969), 820.
[29]. Zhu, L.; Cheng, S. Z. D.; Calhoun, B. H.; Ge, Q.; Quirk, R. P.; Thomas, E. L.; Hsiao, B. S.; Yeh, F.-J.; Lotz B., Polymer 42(2001), 5829.
[30]. Cohen, R. E.; Cheng, P. L.; Douzinas, K.; Kofinas, P.; Berney, C. V. Macromolecules, 23(1990), 324.
[31]. Hamley, I. W.; Fairclough, J. P. A.; Ryan, A. J.; Bates, F. S.; Towns-Andrews, E. Polymer 37(1996), 4425.
[32]. Massa MV, Carvalho JL, Dalnoki-Veress K European Physical Journal E 12(2003),111.
[33]. Massa etal Physical Review Letters 80(1998), 3771.
[34]. Massa , delnoki-veress, Physical Review Letters 92(2004): Art. No. 255509
[35]. Reiter G Physical Review Letters 87: Art. No. 186101 2001
[36]. A. Schönhals, H. Goering, Ch Schick, B. Frick, R. Zorn Eur.Phys..J 12(2003) 173
[37]. E.hempel etal J.Non-Cryst. Solids(2006) in press.
[28]. Jordan EF, Feldeise.DW, Wrigley AN, J.Polym.Sci.,Pt, A-1,9(1971),1835
[39]. Jordan EF, Arthymys.R, Speca A, Wrigley AN, J.Polym.Sci.Pt-A1,9(1971),3349.
[40]. 5. Hempel, E; Budde, H; Horing, S; Beiner, M, Thermochimica Acta, 432(2005)254.
[41]. Keller A, Pedemont.E, Willmouth.FM Nature, 225(1970),538
[42]. Pakula T, Saijo K, Kawai H, Hashimoto T, Macromolecules 18(1985),1294
[43]. Okamoto S, Saijo K, Hashimoto T, Macromolecules. 27(1994), 5574

[44]. Karl Amundson, Eugene Helfand, Xina Quan, Steven D. Hudson, and Steven D. Smith, Macromolecules 27(1994), 6559

[45]. Grigorova T, Pispas S, Hadjichristidis N, Thurn-Albrecht T, Macromolecules 38 (2005)7430

[46]. Picture courtesy: Optics and molecular materials, Helsinki University of Technology

[47]. Zhang YM, Wiesner U, Spiess HW, Macromolecules, 28(1995),778.

[48]. Koppi KA, Tirrell M, Bates FS, Almdal K, Colby RH J.Phys.2(1992) 1941-1959.

[49]. Chen ZR, Kornfield JA, Polymer, 39(1998), 4679.

[50]. Pakula T, Floudas G in Block copolymers, Calleja,Roslaniec.Z(Eds), Mercel Dekker Inc., New York.

[51]. Lee.K.S. and Wegner G., Polymer 28(1987) 889

[52]. Lee.K.S. and Wegner G., Makromol.chemie. Rapid.comm. 6(1985) 203

[53]. G.R.Strobl,R.Eckel, J.Polym.Sci.,Polym.Phy.Ed.14(1976)913

[54]. Darko.C. Master thesis, Dept. of Polymer Physics, Martin-Luther university, Halle-Wittenberg, Germany.

[55]. R.G.Snyder S.L.Hsu S.Krimm, Spectrochimica acta 34A(1978),395

[56] Ruzette AVG, Banerjee P, Mayes AM, Pollard M, Russell TP, Jerome R, Slawecki T, Hjelm R, Thiyagarajan P, Macromolecules 31(1998),8509.

[58] H. W. S. Hsieh, B. Post, and H. Morawetz, J. Polym. Sci., Polym. Phys. Ed. 14(1996), 1241.